

Effective Field Theory for Few-Nucleon Systems

Paulo F. Bedaque

Nuclear Science Division, Lawrence Berkeley National Laboratory,
Berkeley, CA 94720

Ubirajara van Kolck

Department of Physics, University of Arizona,
Tucson, AZ 85721

RIKEN BNL Research Center, Brookhaven National Laboratory,
Upton, NY 11973

KEYWORDS: effective field theory, chiral perturbation theory, nuclear physics, few-body systems

ABSTRACT:

We review the effective field theories (EFTs) developed for few-nucleon systems. These EFTs are controlled expansions in momenta, where certain (leading-order) interactions are summed to all orders. At low energies, an EFT with only contact interactions allows a detailed analysis of renormalization in a non-perturbative context and uncovers novel asymptotic behavior. Manifestly model-independent calculations can be carried out to high orders, leading to high precision. At higher energies, an EFT that includes pion fields justifies and extends the traditional framework of phenomenological potentials. The correct treatment of QCD symmetries ensures a connection with lattice QCD. Several tests and prospects of these EFTs are discussed.

With permission from the Annual Review of Nuclear and Particle Science. Final version of this material is scheduled to appear in the Annual Review of Nuclear and Particle Science Vol. 52, to be published in December 2002 by Annual Reviews (<http://AnnualReviews.org>).

CONTENTS

INTRODUCTION	2
<i>Why effective theories?</i>	2
<i>What is an effective theory?</i>	2
<i>How?</i>	4
EFT WITHOUT EXPLICIT PIONS	5
<i>The two-nucleon system and the non-trivial fixed point</i>	5
<i>The three-body system and the limit cycle</i>	15
EFT WITH EXPLICIT PIONS	23
<i>Chiral symmetry and Chiral Perturbation Theory</i>	24
<i>The two-nucleon system</i>	26

<i>Three- and four-nucleon systems</i>	40
<i>Processes with external probes</i>	43
<i>Connection with lattice QCD</i>	48
OUTLOOK	49
<i>More-nucleon systems</i>	50
<i>Conclusion</i>	50

1 INTRODUCTION

1.1 *Why effective theories?*

Nuclear systems have often been described as pathologically complicated. The forces between the constituent nucleons are strong and non-central and the relatively small binding found in nuclei results from detailed cancellations between much larger contributions. Adding the fact that the basic interaction among nucleons is not completely known, especially at short distances, and the problems involved in the numerical solution of the Schrödinger equation for systems with many fermions, one can understand why nuclear structure remains an unsolved problem after decades of intense effort. This seems even more frustrating when one remembers that all nuclear processes are encoded in the QCD Lagrangian and parameter-free predictions could, in principle, be obtained. Despite all these difficulties enormous progress has been made throughout the years by the use of models capturing different aspects of nuclear phenomena. One dissatisfying aspect of these models however is their basically *ad hoc* nature and the presence of uncontrolled approximations. These models are not derived from any basic principle (and certainly not from QCD) and contain information coming from decades of trial and error hidden behind apparently arbitrary choices of some contributions over others. Each new improvement involves the same process of educated guesses and one is never sure of what a reasonable error estimate would be. Effective field theories (EFTs) are useful by providing a systematic expansion in a small parameter that organizes and extends previous phenomenological knowledge about nuclear processes and by providing a rigorous connection to QCD. They also help with more technical but important issues that have plagued nuclear physics in the past, like gauge invariance, “off-shell” effects and relativistic corrections, by borrowing heavily from the arsenal of field theory.

1.2 *What is an effective theory?*

Most of the uncertainty in nuclear processes comes from the short-distance interactions ($\lesssim 1$ fm) between two or more nucleons (and photons, leptons). Even when one is interested only in low-energy phenomena, the short-distance contributions can be important. In perturbation theory, for instance, the influence of short-distance physics on low-energy observables appears in the existence of ultraviolet-divergent integrals, that is, in the dominance of high-momentum modes over the small-momentum ones. Sensitivity of large-distance observables on short-distance physics is not an unusual situation in physics, it is in fact pervasive in many fields. One way of dealing with it is to model the short-distance physics and solve the problem from a microscopic approach. In the case of nuclear systems this would lead either to a calculation of nuclear processes directly from QCD (which is currently impossible and would be, even if possible,

a highly inefficient way of approaching the problem) or to the use of meson-exchange/quark/skyrmion/... models. Another approach is the use of effective theories (1)¹. Before introducing the particular case used in nuclear physics, let us consider effective theories in general.

Suppose we want to study the low-energy behavior of a system described by some theory that we will call the “fundamental” theory. In the path-integral formalism, we can imagine integrating over the high-momentum modes $k < \Lambda$, where the scale Λ is chosen to be much larger than the momentum scale we want to study. The result of this partial integration over the high-momentum modes will be a complicated Lagrangian containing an infinite number of terms. This Lagrangian, called the effective Lagrangian, will also be, in general, non-local, but this non-locality, arising from the momenta $k < \Lambda$ will be restricted to a spatial scale $\lesssim 1/\Lambda$. One can thus expand those interaction terms in a Taylor series on ∂/Λ , where ∂ stands for a derivative of the fields. The coefficients of this expansion do not depend on the soft momenta carried by the field of the effective theory and describe the hard physics within the scale $1/\Lambda$. They are, however, functions of Λ (the coupling constants “run”). The soft ($k < \Lambda$) and hard ($k > \Lambda$) physics are factorized in the effective Lagrangian. These effective-Lagrangian coefficients are usually called “low-energy constants” (LECs) since they encode all we need to know about the fundamental theory in order to compute low-energy observables. Notice that, up to this point, no approximation was made and the effective Lagrangian contains exactly the same information as the fundamental one. Calculations of observables done using the effective Lagrangian will contain two sources of Λ dependence. One is the implicit dependence contained in LECs, the other appears in the cutoff that should be used in those computations. These two sources of Λ dependence, by construction, cancel each other.

One may wonder what the advantage is in separating the integration over momentum modes in two steps. The answer to this question depends on the particular situation in hand. In problems where the integration over the high-momentum modes can be explicitly accomplished the effective Lagrangian is a bookkeeping device that allows us to perform approximations in a very efficient way. That is the case, for instance, of non-relativistic QED (2), heavy-quark effective theory (3), and high-density QCD chiral perturbation theory (4). In other cases, as the nuclear systems considered here, we will not be able to explicitly integrate the high-momentum modes. We can however determine the effective Lagrangian by a combination of self-consistency requirements and experimental data. We start by considering the most general Lagrangian consistent with the symmetries of the underlying theory. This Lagrangian contains an infinite number of arbitrary constants. For a fixed Λ , different values of the LECs describe different underlying theories. Just one set of these values will make our low-energy theory reproduce the same observables as the fundamental theory. We then resort to an approximation scheme: we expand the low-energy observables in powers of the small parameter $Q/\Lambda \ll 1$, where Q is a low-energy scale like the momenta of the external particles, light masses, *etc.* Now the factorization between high- and low-momentum contributions comes in handy. Instead of using

¹ The term “effective theories” has also other meanings besides the specific one assumed in this review. “Effective Lagrangian” sometimes is meant as the one including all quantum corrections. Other times the term “effective theory” is used to describe any model useful at low energies, whether or not there is a separation of scales and a rigorous expansion in powers of the momentum.

the full effective Lagrangian with its infinite number of terms we can argue that, *at a given order in the Q/Λ expansion*, only a finite number of them will contribute, since the remaining terms will include many powers of $\partial/\Lambda \sim Q/\Lambda$. This way we are left with a much simpler Lagrangian, with a finite (and hopefully small) number of coefficients that can be determined from some experimental data (or from the fundamental theory, if possible, or models) and used to predict others. Increasing the order in Q/Λ of a calculation will increase its precision but may also bring other LECs that will have to be determined by experiment. The precise argument connecting the order of the expansion in powers of Q/Λ and the terms in the effective Lagrangian that need to be included at that order (called “power counting”) varies case by case but always include two steps. The first one is to estimate the size of diagrams, given the size of the LECs appearing on the vertices, and it is simply done by dimensional-analysis arguments. The second one is to estimate the size of the LECs themselves. For that we first determine their running, that is, their dependence on Λ , by requiring physical observables to be Λ independent (at the order in Q/Λ we are working). The information about the evolution of the LECs is not by itself enough to determine them since we do not know their initial conditions. Although for some particular value of Λ one LEC might be passing through zero, this is very unlikely. We assume that a typical size for a LEC $C(\Lambda)$ is $C(\Lambda) \sim C(2\Lambda) - C(\Lambda)$, that is, the LECs should have the same order of magnitude as the size of their running. In perturbative settings this principle amounts to little more than dimensional analysis, and is known as “naive dimensional analysis” (5). Strictly, this provides only a reasonable lower bound, so one should be aware of possible violations of this principle. This estimate, of course, is used only in arguing that some terms in the effective Lagrangian will have a negligible effect and can be dropped. The values of the LECs actually kept in the calculation are determined by experimental data. Notice that, for a given set of symmetries and low-energy degrees of freedom, there is no guarantee that the effective Lagrangian can be truncated at any order in Q/Λ , that is, there is no guarantee that a consistent power counting can be found.

The version of the EFT method sketched above is sometimes called the “Wilsonian” effective theory. Another version of the same basic idea, identical in spirit but differing in detail is given by the “continuum” effective theory (3). There, we construct the effective theory in such a way as to reproduce the same vertices and propagators as the full theory at *low energy*. The two theories differ in the ultraviolet region but this difference can always be absorbed in the values of the LECs. The technical advantage over the Wilsonian approach resides on being able to integrate over all momenta (used in conjunction with dimensional regularization), and not only over $k < \Lambda$, which makes it simpler to maintain gauge, chiral and spacetime symmetries, and to avoid power-law divergences that sometimes complicate power counting.

1.3 How?

EFTs can be used in a few different ways in nuclear physics. Historically, the first one was to set the separation scale Λ around the ρ -meson mass and keep as low-energy degrees of freedom the pions and the nucleons² (and maybe the Δ

²Since energies are measured from the ground state *with a given baryon number*, slow nucleons, despite carrying large rest-mass energy, should be considered low-energy degrees of freedom.

isobars), as well as photons and leptons (6, 7, 8, 9, 10, 11). This approach builds on and extends the success of Chiral Perturbation Theory (ChPT) in the mesonic and one-baryon sectors. It shares with nuclear potential models the fact that it describes non-relativistic nucleons interacting through a potential, but it also brings a number of ingredients of its own, such as a small expansion parameter, consistency with the chiral symmetry of QCD, and systematic and rigorous ways of including relativistic corrections and meson-exchange currents.

Another way of applying EFT ideas in nuclear physics is made possible by the existence of shallow bound states, that is, binding energies much below any reasonable QCD scale (12, 13, 14, 15). We can then set Λ around the pion mass and keep as low-energy degrees of freedom only the nucleons (and photons, leptons). At least in the case of two- and three-body systems the bound states will be within the range of validity of this simpler theory. This “pionless” effective theory can be considered as a formalization and extension of the old effective-range theory (ERT) (16) and the work on “model-independent results” in three-body physics (17). The new features, besides the existence of a small parameter on which to expand, appear in a number of new short-distance contributions describing exchange currents and three-body forces, as well as in relativistic corrections, that are transparent in this approach. An extra bonus is the possibility of deriving analytic, high-precision expressions for many observables that previously could only be obtained after non-trivial numerical work.

In Sects. 2 and 3 we will review these two approaches in few-nucleon systems, emphasizing qualitative aspects of recent developments. In Sect. 4 we present an outlook, including other approaches that are being developed for larger nuclei. Some reviews have already appeared covering applications of EFT ideas to nuclear physics, with different emphasis from the present one (18). Many developments of the last couple of years are described in Ref. (19).

2 EFT WITHOUT EXPLICIT PIONS

2.1 The two-nucleon system and the non-trivial fixed point

2.1.1 Two-nucleon scattering

Let us now apply the ideas outlined in the previous section to the specific case of two nucleons with momentum k below the pion scale $k < m_\pi$. More details can be found in Ref. (15). We start by writing the most general Lagrangian involving only two nucleons (electroweak external currents will be included later). A system with two nucleons with zero angular momentum $L = 0$ can exist in a spin singlet (1S_0) or spin triplet (3S_1) state so there are two independent interactions with no derivatives,

$$\mathcal{L} = N^\dagger (i\partial_0 + \frac{\vec{\nabla}^2}{2M} + \dots) N - C_{0t} (N^\dagger P_t N)^2 - C_{0s} (N^\dagger P_s N)^2 + \dots, \quad (1)$$

where

$$\begin{aligned} P_t^i &= \frac{1}{\sqrt{8}} \sigma_2 \sigma^i \tau_2, \\ P_s^A &= \frac{1}{\sqrt{8}} \tau_2 \tau^A \sigma_2 \end{aligned} \quad (2)$$

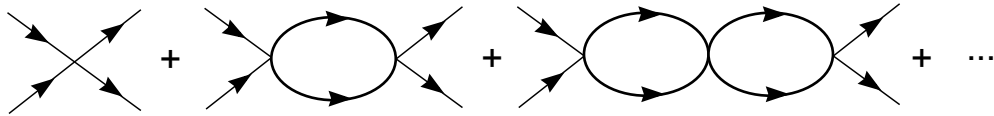


Figure 1: Graphs contributing to the LO NN scattering amplitude.

are the projectors in the triplet and singlet spin-isospin states (σ 's act on spin space, τ 's on isospin space), M is the nucleon mass and N the nucleon field. The dots in Eq. (1) stand for terms with more derivatives that, as we will argue later, will be subdominant.

The nucleon-nucleon (NN) scattering amplitude can be written in terms of the phase shift δ as

$$\begin{aligned} T &= \frac{4\pi}{M} \frac{1}{k \cot \delta - ik} \\ &= \frac{4\pi}{M} \frac{1}{-\frac{1}{a_s} + \frac{r_{0s}}{2} k^2 + \dots - ik} \end{aligned} \quad (3)$$

It can be shown that for potentials of range $\sim R$ ($R \sim 1/m_\pi$ in our case), $k \cot \delta$ is an analytic function around $k = 0$ and that it has a cut starting at $k^2 \sim 1/R^2$, so it is well approximated by a power series as shown in the last line of Eq. (3). The parameter a_s (r_{0s}) is called the singlet scattering length (singlet effective range). For notational simplicity we specialize for now on the spin singlet channel.

The graphs contributing to NN scattering generated by the Lagrangian in Eq. (1) are shown in Fig. (1). The L -loop graph factorizes into a power,

$$L\text{-loop graph} \sim (c\Lambda - ik)^L, \quad (4)$$

each one containing a linearly divergent piece and the unitarity cut ik (in the center-of-mass system with total energy k^2/M). The loop integral is linearly divergent and the coefficient c is dependent on the particular form of the regulator used, that is, the particular form the high-momentum modes are separated from the low-momentum ones. Using a sharp momentum cutoff, for instance, we have $c = 2/\pi$, using dimensional regularization (DR), $c = 0$. The sum of all graphs in Fig. (1) is a geometrical sum giving

$$T = \frac{4\pi}{M} \frac{1}{-\frac{4\pi}{MC_{0s}} + c\Lambda - ik}. \quad (5)$$

We see then that terms shown explicitly in Eq. (1) reproduce the first term of the effective range expansion. The addition of terms with more derivatives will reproduce further terms in the effective range expansion.

We can learn some important lessons from this simple calculation. Let us consider two separate situations.

Natural case: For a generic potential with range R , the effective-range parameters typically have similar size $a \sim r_0 \sim R$. Using DR, C_0 can be chosen to

be $C_0 = 4\pi a/M$ (this choice is called minimal subtraction). The effective theory is valid for $k < 1/R$ and, in this range, T can be expanded as

$$T = \frac{4\pi}{M} \left(-a + ik a^2 + \left(\frac{a^2 r_0}{2} + a^3 \right) k^2 + \dots \right). \quad (6)$$

Since $C_0 \sim a$, there is a one-to-one correspondence between the order in the ka expansion, the number of C_{0s} vertices and the number of loops in a graph. The leading order (LO) is given by one tree-level diagram, the next-to-leading order (NLO) by the one-loop diagram, next-to-next-to-leading order (N²LO) by the two-loop diagram involving C_0 and one tree-level diagram with a two-derivative vertex (not shown in Eq. (1)), and similarly for higher orders. We have then a *perturbative* expansion, even though the microscopic potential can be arbitrarily strong. If one uses a cutoff regulator the situation is slightly more complicated. Choosing $\Lambda \sim 1/R \sim 1/a$ we note that the most divergent piece of the multi-loop graphs is as large as the tree-level graph and must be resummed to all orders, while the energy-dependent part containing powers of ikC_0 is suppressed. The pieces that need to be resummed at leading order merely renormalize the constant C_0 . The one-to-one correspondence between the order in the ka expansion and the number of loops is lost in any but the DR with minimal subtraction renormalization/regularization scheme. The technical advantages arising from the use of DR and renormalization theory in this perturbative setting was used in the study of dilute gases with short-range interactions in Ref. (20).

Unnatural case: In the nuclear case the scattering lengths of the two S-wave channels are much larger than the range of the potential. The 1S_0 (neutron-proton) scattering length a_s is $a_s = -23.714$ fm and the scattering length of the triplet (deuteron) channel 3S_1 is $a_t = 5.42$ fm, corresponding to momentum scales of $1/a_s = 8.3$ and $1/a_t = 36$ MeV, respectively. Those scales are much smaller than the pion mass, $m_\pi \simeq 140$ MeV, defining the range of the nuclear potential³. Actually, we will see later that the potential due to pion exchange is too weak to describe the low-energy phase shifts, and the physics corresponding to the large scattering lengths occurs at the QCD scale $M_{QCD} \sim 1$ GeV, what makes the discrepancy between nuclear and QCD scales even more startling. The origin of the fine-tuned cancellations leading to the disparity between the underlying scale and the S-wave scattering lengths (and deuteron binding energy) is presently unknown. It does not appear in any known limit of QCD like the chiral limit ($m_q \rightarrow 0$) or large number of colors ($N_c \rightarrow \infty$). We will just assume that this cancellation happens, track the dependence of observables on the new soft scale $1/a_{s,t}$ and perform our low-energy expansion in powers of $kR \ll 1$ while keeping the full dependence on $ka_{s,t} \sim 1$. The singlet NN scattering amplitude, for instance, will be expanded as

$$T = -\frac{4\pi}{M} \left(\frac{a_s}{1 + ika_s} + \frac{k^2 a_s^2 r_{0s}}{2} \frac{1}{(1 + ika_s)^2} + \dots \right). \quad (7)$$

It is a little challenging to reproduce an expansion of this form in the EFT. If one uses a momentum cutoff, for instance, the constant C_{0s} has to be chosen to

³Alkali atoms used in cold atomic traps frequently have scattering lengths much larger than their sizes. They can be made even larger by the use of a carefully tuned external magnetic field (Feshbach resonances). All the ideas and formalisms developed to deal with this fact in the nuclear domain can and have already been used to study the physics of atomic traps (21, 22).

be $C_{0s} = (4\pi/M)(1/a_s + c\Lambda)$. The one-loop graph is then suppressed compared to the tree-level one by a factor $\sim MkC_{0s} \sim k/\Lambda$ and one would naively imagine that the leading-order contribution is given solely by the tree-level graph. But there are cancellations between the graphs in Fig. (1) and all these graphs need to be taken into account to reproduce the expansion of T above (13,14). In the NN scattering case considered here it is not difficult to see which graphs have to be included at each order, but in more complex situations this can be extremely tricky. A more convenient way to proceed is to use a renormalization prescription that shifts contributions from high-momentum modes to the LECs in such a way as to eliminate this “accidental” cancellations between different diagrams. One can determine which diagrams contribute at each order on a diagram-by-diagram basis (manifest power counting). One way to do that is to use DR with a “power divergence subtraction” (PDS) (23)⁴. In this scheme, we add and subtract to the denominator of the bubble sum in Eq. (5) an amount $M\mu/4\pi$, where μ is an arbitrary scale, and absorb the subtracted term in a redefinition of the constant $C_{0s}(\mu)$, that now is a function of μ . We have for the LO amplitude

$$T = -\frac{4\pi}{M} \frac{1}{\frac{4\pi}{MC_{0s}(\mu)} + ik + \mu}. \quad (8)$$

The constants $C_{0s}(\mu)$ is now chosen to be

$$C_{0s}(\mu) = \frac{4\pi}{M} \frac{1}{\frac{1}{a_s} - \mu}, \quad (9)$$

in order to reproduce the LO piece of the expansion in Eq. (7). The explicit dependence on μ cancels against the implicit dependence contained in $C_{0s}(\mu)$. The point of this rearrangement is that if μ is chosen so that $\mu \sim 1/a_s$, $C_{0s}(\mu) \sim 4\pi/M\mu$ and the contribution of all diagrams in the bubble sum are of the same order, justifying the need to resum them. Let us see how this works in some detail. Denoting the soft scales $1/a_s$, μ and k collectively by Q , the tree-level diagram is of the order $C_{0s} \sim 4\pi/M\mu$. The one-loop graph contains two powers of C_{0s} , two nucleon propagators, each one counting as $1/(k^2/M) \sim M/Q^2$, and a loop integral with three powers of momentum ($\sim Q^3$), one of energy ($\sim Q^2/M$) and the usual factor of $1/4\pi$ from the loop integration, for a total of $(4\pi/MQ)^2(M/Q^2)^2Q^5/M \sim 4\pi/MQ$. Thus the one-loop diagram has the same size of the tree-level graph. The same occurs for the remaining diagrams and they all have to be resummed. It is interesting to note that this reshuffling of contributions between the divergent loop and the LECs amounts to subtracting the poles $1/(D-2)$, where D is the number of spatial dimensions, that would exist in two space dimensions. One can easily go to higher orders and include terms with derivatives in the Lagrangian. A simple calculation (again, subtracting the pole occurring in two spatial dimensions) leads to expressions for all the LECs in terms of the effective-range parameters (and of the arbitrary scale μ). For instance, denoting by C_{2n} the coefficient of operators with $2n$ derivatives,

$$C_{2s} = \frac{4\pi}{M} \frac{r_{0s}}{2} \left(\frac{1}{\frac{1}{a_s} - \mu} \right)^2, \quad (10)$$

⁴Other schemes also solve this problem (24).

$$C_{4s} = \frac{4\pi}{M} \left(\frac{r_{0s}^2}{4} \left(\frac{1}{\frac{1}{a_s} - \mu} \right)^3 + \frac{r_{1s}^3}{2} \left(\frac{1}{\frac{1}{a_s} - \mu} \right)^2 \right), \quad (11)$$

where r_{1s} is the coefficient of the third term of the effective-range expansion (“shape parameter”).

The β -function describing the evolution of the dimensionless coupling $\hat{c}_{0s} \equiv -M\mu C_{0s}/4\pi$ is

$$\mu \frac{\partial}{\partial \mu} \hat{c}_{0s}(\mu) = \hat{c}_{0s}(\mu) (1 - \hat{c}_{0s}(\mu)) \quad (12)$$

Note the existence of two fixed points (23, 25), the trivial (perturbative) one at $\hat{c}_{0s} = 0$ and a non-trivial one at $\hat{c}_{0s} = 1$. For $\mu \ll 1/|a_s|$, as appropriate to the natural case discussed above, \hat{c}_{0s} is close to the trivial fixed point. Diagrams involving more C_{0s} vertices are suppressed by powers of $\hat{c}_{0s} \ll 1$ and the system is perturbative. The value $\hat{c}_{0s} \sim \mu a_s$ corresponds to the naive-dimensional-analysis one and the effects of the C_{0s} operator become smaller at lower energies (the operator is *irrelevant*). On the other hand, for values of $\mu \sim 1/|a_s|$ or larger, as adequate to the fine-tuned case discussed here, the flow is close to the non-trivial fixed point. Since $\hat{c}_{0s} \sim 1$, the addition of more C_{0s} vertices is not suppressed and all graphs containing only this vertex should be resummed. The dimensionless coupling \hat{c}_{0s} goes from the naive-dimensional-analysis value $\hat{c}_{0s} \sim \mu a_s$ to $\hat{c}_{0s} \sim 1$ and its effects do not go away in the infrared (*marginal* operator).

Since the 3S_1 scattering length is also unnaturally large (and consequently the deuteron is unnaturally shallow), the same power counting used in the singlet channel applies also to the triplet channel. NN scattering in this channel is more complicated because nuclear forces, being non-central, mix it with the 3D_1 channel. There are new operators, starting with two derivatives, describing this mixing. Their coefficients are determined from an expansion of mixing angle analog to Eq. (7). Also, the LECs are usually determined by matching to an effective range expansion centered around the deuteron pole, as opposed to the one centered around $k = 0$ as is done in the singlet channel. The 3S_1 NN amplitude is parameterized as

$$T = \frac{4\pi}{M} \frac{1}{-\gamma + \frac{\rho(k^2 + \gamma^2)}{2} + \dots - ik} \quad (13)$$

where γ^2/M is the deuteron binding energy and ρ the effective range parameter. Explicit expressions for the leading terms in the Lagrangian and numerical values for the LECs can be found in Ref. (15).

The inclusion of external currents (photons, neutrinos, ...) is straightforward. All terms involving nucleons and the new fields or currents should be included, as long as they satisfy the symmetries of the underlying theory. In the case of photons, some of these terms are just those required by gauge invariance and are determined by minimally coupling the photon to the nucleon Lagrangian. Their coefficients are thus fixed by NN scattering data and gauge invariance. There are also terms that are gauge invariant by themselves and whose coefficients are *not* determined by NN scattering data alone. They represent the physics of exchange currents, quark effects, *etc.*, and need to be determined through some extra piece of experimental data. To perform the low-energy expansion though, it is necessary to have an *a priori* estimate of their size. This estimate is obtained by using the fact that observables should be independent of the cutoff

(or μ if using DR), at least up to the order one is computing. Consider some two-nucleon operator of the form $X = C_{2n}^X N^\dagger N^\dagger \Gamma_X \vec{\partial}^{2n} N N$, where Γ_X is some tensor in spin-isospin space. Its matrix element on two-nucleon states is given by the diagrams involving the operator X “sandwiched” between two two-nucleon scattering amplitudes and by one-loop one-body diagrams that do not involve X . Typically the one-body diagram is not divergent and does not introduce any μ dependence⁵ so the remaining graphs have to be μ independent by themselves. We have to make a distinction now between the cases where the operator X connects two S -wave states, two non- S -wave states, or one S -wave and one non- S -wave state. In the first case renormalization-group invariance of the two-nucleon matrix element of X implies

$$\mu \frac{\partial}{\partial \mu} C_{2n}^X(\mu) \left(\frac{T}{C_0(\mu)} \right)^2 = 0, \quad (14)$$

where T is the LO NN scattering matrix, which is μ independent. From that it follows that $C_{2n}^X(\mu)$ scales as $\sim (\mu - 1/a)^{-2}$. Similarly, for the case where X connects one S -wave or no S -wave states $C_{2n}^X(\mu)$ scales as $\sim (\mu - 1/a)^{-1}$ and $\sim (\mu - 1/a)^0$, respectively. Using dimensional analysis to fix the powers of Λ we then have

$$C_{2n}^X(\mu) \sim \frac{1}{M(1/a - \mu)^\alpha} \frac{1}{\Lambda^{2n+1-\alpha}}, \quad (15)$$

where α is the number of S -wave states the operator X can connect (either 0, 1 or 2).

In a nutshell, the power counting rules valid for the two-nucleon system are (13, 14, 23, 15):

$$\begin{aligned} \text{fermion line} &\rightarrow M/Q^2 \\ \text{loop} &\rightarrow \frac{Q^5}{4\pi M} \\ \vec{\partial} &\rightarrow Q \\ \partial_0 &\rightarrow Q^2/M \\ C_{2n} &\rightarrow \frac{4\pi}{M\Lambda^n Q^{n+1}} \\ C_{2n}^X &\rightarrow \frac{4\pi}{M\Lambda^{2n+1-\alpha} Q^\alpha}, \end{aligned} \quad (16)$$

where C_{2n} is the coefficient of the two-nucleon interaction with $2n$ derivatives, C_{2n}^X is the coefficient of a two-nucleon operator with external current X and $2n$ derivatives, and Λ is the high-energy scale $\Lambda \sim m_\pi$.

Using this rule we can determine the contributions to NN scattering at any given order. At LO, for instance, we have the series of diagrams shown in Fig. (1), with all the vertices containing no derivative. That is the only non-perturbative resummation necessary. At NLO we have the insertion of one C_2 operator in a chain of C_0 operators. At N²LO we have two insertions of C_2 and one insertion of C_4 , and so on. The resulting 3S_1 phase shift, for example, is shown in Fig. (2), and compared to the Nijmegen phase-shift analysis (PSA) (26). Analytic expressions for the phase shifts can be found in Ref. (15). They suggest convergence for momenta $k \lesssim 100$ MeV, as it is reasonable for an EFT without explicit pions.

⁵One exception is the two-nucleon, no-external-current C_4 operator whose renormalization is driven by C_2 . This explains the apparent discrepancy between Eq. (10) and Eq. (15).

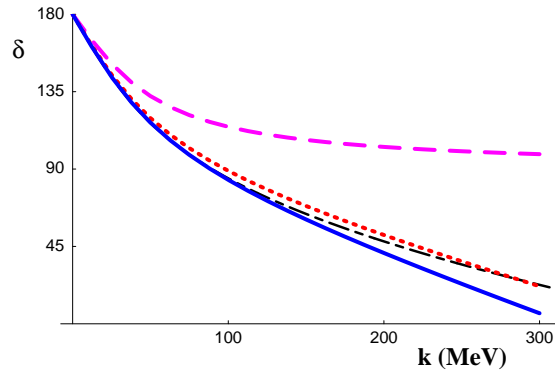


Figure 2: 3S_1 NN phase shift (in degrees) as function of the center-of-mass momentum. The LO result is the dashed (purple) line, the N^2 LO the dotted (red) line and N^4 LO the thick (blue) solid curve. The dot-dashed line is the Nijmegen PSA. From Ref. (15), courtesy of M. Savage.

Electromagnetic effects in proton-proton scattering were considered in the EFT approach in Ref. (27).

Up to this point we have considered only NN scattering, where the predictive power of the pionless EFT is very small. We were able however to determine many LECs using scattering data and understand the effects of the fine-tuning on the S -wave channels. We now apply the formalism developed above to the computation of form factors and processes involving external currents. We will omit the diagrams needed to be computed and the explicit analytic expressions that are always available in the two-nucleon sector. They can be found in the literature cited.

2.1.2 Electromagnetic form factors of the deuteron

The matrix element of the electromagnetic current on the deuteron has the non-relativistic parameterization

$$\begin{aligned} \langle p', \epsilon^j | J_{em}^0 | p, \epsilon^i \rangle &= e \left[F_C(q^2) \delta_{ij} + \frac{1}{2M_d^2} F_Q(q^2) \left(q_i q_j - \frac{1}{3} q^2 \delta_{ij} \right) \right] \left(\frac{E + E'}{2M_d} \right), \\ \langle p', \epsilon^j | \vec{J}_{em}^k | p, \epsilon^i \rangle &= \frac{e}{2M_d} \left[F_C(q^2) \delta_{ij} (p + p')^k + F_M(q^2) \left(\delta_j^k q_i - \delta_i^k q_j \right) \right. \\ &\quad \left. + \frac{1}{2M_d^2} F_Q(q^2) \left(q_i q_j - \frac{1}{3} q^2 \delta_{ij} \right) (p + p')^k \right], \end{aligned} \quad (17)$$

where $|p, \epsilon^i\rangle$ is the deuteron state with momentum p and polarization ϵ^i , M_d is the deuteron mass, $q = p' - p$ and the form factors are normalized such that $F_C(0) = 1$ (deuteron charge), $eF_M(0)/2M_d = \mu_D$ (deuteron magnetic moment) and $F_Q(0)/M_d^2 = \mu_Q$ (deuteron quadrupole moment).

At LO and NLO the computation of $F_C(q^2)$ involves only the constants C_{0t} and C_{2t} and is identical to the ERT calculation. At N^2 LO a one-body term describing the nucleon charge mean square radius ($\langle r^2 \rangle_N$) appears, which is the first deviation from ERT (15). Formally there are also relativistic corrections, but they are suppressed by powers of Q/M as opposed to Q/m_π , and are numerically

small. Still they can be readily computed in EFT. Defining the deuteron charge mean square radius by $\langle r^2 \rangle_d \equiv 6(dF_C/dq^2)$, one finds

$$\langle r^2 \rangle_d = \langle r^2 \rangle_N + \frac{1}{1 - \gamma\rho} \frac{1}{8\gamma^2} + \frac{1}{32M^2} = 4.565 \text{ fm}^4, \quad (18)$$

to be compared with the experimental value $\langle r^2 \rangle_d = 4.538 \text{ fm}^4$.

The magnetic form factor $F_M(q^2)$ at LO and NLO is simply the electric form factor $F_C(q^2)$ multiplied by the isoscalar nucleon magnetic moment $\kappa_n + \kappa_p$, except for a new two-body term appearing at NLO without an ERT analog,

$$\mathcal{L} = -eL_2 i\epsilon^{ijk} (NP_i N)^\dagger (NP_j N) B_k + \text{h.c.} \quad (19)$$

L_2 can be determined through the experimental value of the deuteron magnetic moment and, using this value, the momentum dependence of $F_M(q^2)$ is then predicted.

The $F_Q(q^2)$ form factor involves a transition between the S - and D -wave components of the deuteron. At LO its value is determined by a S - to D -wave transition operator whose coefficient is extracted from the asymptotic D/S ratio of the deuteron, $\eta_{D/S}$. At NLO there is a new two-body term

$$\mathcal{L} = -eC_Q (NP_i N)^\dagger (NP_j N) \left(\nabla^i \nabla^j - \frac{1}{3} \nabla \delta^{ij} \right) A^0, \quad (20)$$

whose coefficient C_Q can be fitted to the experimental deuteron quadrupole moment. At N²LO the only contribution comes from the finite size of the nucleon charge distribution $\langle r^2 \rangle_N$. The value of $F_Q(0)$ is then a fit, but the momentum dependence is an EFT prediction. The presence of a counterterm not determined by NN scattering at NLO indicates that μ_Q is sensitive at the $\sim 10\%$ level to short-distance physics not determined by NN scattering. That is probably the reason different potential-model calculations underpredict μ_Q by $\simeq 5\%$.

2.1.3 Deuteron polarizabilities and Compton scattering

The deuteron is a very loose bound state so it is no surprise that its electric polarizability depends mostly on the large-distance part of its wave-function. Consequently, a model-independent prediction can be made with a high degree of accuracy. The electric (magnetic) scalar deuteron polarizabilities α_{E0} (α_{M0}) are defined by

$$\mathcal{L}_{\mathcal{D}} = 2\pi\alpha_{E0} d^{i\dagger} d^i \vec{E}^2 + 2\pi\alpha_{M0} d^{i\dagger} d^i \vec{B}^2, \quad (21)$$

where d^i is a canonically normalized deuteron field.

The EFT result for α_{E0} up to N³LO is (15)

$$\alpha_{E0} = \frac{\alpha M}{32\gamma^4} \frac{1}{1 - \gamma\rho} \left(1 + \frac{2\gamma^2}{3M^2} + \frac{M\gamma^3}{3\pi} D_P + \dots \right) = 0.6325 \pm 0.002 \text{ fm}^3, \quad (22)$$

where $D_P = -1.51 \text{ fm}^3$ is a combination of constants describing P -wave two-nucleon interactions and in the last line we used the fact that higher-order computations always build the deuteron wave-function renormalization factor $Z = 1/(1 - \gamma\rho)$ ⁶. The first two-nucleon current operator appears only at N⁵LO.

⁶A modified method counting the effective range parameters as $r_{0s}, \rho \sim 1/Q$ formalizes this observation (28).

Since all the inputs were determined from NN scattering, we expect that any model describing the phase shifts well should make predictions within the estimated error. Indeed a number of models predict $\alpha_{E0} = 0.6328 \pm 0.0017 \text{ fm}^3$.

Magnetic, vector and tensor polarizabilities, and their momentum-dependent analogs were not yet analyzed in the pionless EFT (see below for results using the pionful EFT). However, these polarizabilities determine the amplitude for low-energy Compton scattering off the deuteron, that was analyzed in Ref. (29). The *nucleon* polarizabilities appear already at NLO and Compton scattering can be used to extract the hard-to-measure neutron polarizabilities.

2.1.4 Radiative capture of neutrons by protons

The $n + p \rightarrow d + \gamma$ reaction at low energies is a key ingredient in Big-Bang nucleosynthesis calculations. The amplitude for this process can be expanded in multipoles as

$$\begin{aligned} \mathcal{A} = & ieX_{M1V}\epsilon^{ijk}\epsilon^{*i}k^j\epsilon^k nP^3p + eX_{E1V} n\tau_2\tau_3\sigma_2\vec{\sigma} \cdot \vec{\epsilon}^* pP^i\epsilon^{*i} \\ & + \frac{eX_{M1S}}{\sqrt{2}} nP^i[k^i\vec{\epsilon}^* \cdot \vec{\epsilon}^* - \vec{\epsilon}^* \cdot \vec{k}\epsilon^{*i}]p \\ & + \frac{eX_{E2S}}{\sqrt{2}} nP^i[k^i\vec{\epsilon}^* \cdot \vec{\epsilon}^* + \vec{\epsilon}^* \cdot \vec{k}\epsilon^{*i} - \frac{2}{3}\epsilon^{*i}\vec{k} \cdot \vec{\epsilon}^*]p + \dots, \end{aligned} \quad (23)$$

where n and p are the neutron and proton Pauli spinors, k is the photon momentum and ϵ (ϵ) is the polarization of the deuteron (photon). At low energies the form factor X_{M1V} dominates the cross section by a few orders of magnitude. Its computation at LO is the same as the ERT one and underpredicts the experimental value for thermal neutron capture by 10%. This discrepancy was explained long ago as due to a pion-exchange current contribution (30). In EFT (15) the same effect is encapsulated in the two-nucleon current

$$\mathcal{L} = eL_{M1V}(NP^iN)^\dagger(NP^AN)\delta_{A3}B^i + \text{h.c.}, \quad (24)$$

whose coefficient L_{M1V} can be determined by the cold-capture cross section. The momentum dependence is then predicted. However for photon energies larger than a few MeV the X_{E1V} form factor dominates the cross section. Up to N³LO the computation of X_{E1V} involves only C_{0t} , C_{2t} , the P -wave interaction combination D_P encountered in the polarizability calculation, and L_{M1V} fitted at threshold. At N⁴LO some relativistic effects and a new term appears (31),

$$\mathcal{L} = eL_{E1V}(NP^iN)^\dagger(N(\vec{\nabla}_i\tilde{P}_{jA} - \overleftarrow{\nabla}_j\tilde{P}_{iA})N)\delta_{A3}E^j, \quad (25)$$

where $\tilde{P}_{iA} = \sigma_2\sigma_i\tau_2\tau_A/\sqrt{8}$, which is fitted using data for the inverse reaction $d + \gamma \rightarrow n + p$. The resulting cross section for the photodissociation of the deuteron is shown in Fig. (3), and compared to data (32). The estimated error is of the order $(Q/m_\pi)^5 \sim 1\%$. These precise, analytical computations are particularly useful for Big-Bang nucleosynthesis codes.

A set of polarization observables in the $n + p \rightarrow \gamma + d$ reaction was analysed in Ref. (33).

2.1.5 Neutrino-deuteron scattering and proton-proton fusion

A complete set of reactions involving (anti-)neutrino breakup of the deuteron were computed in the pionless EFT approach (34). Proton-proton fusion and the

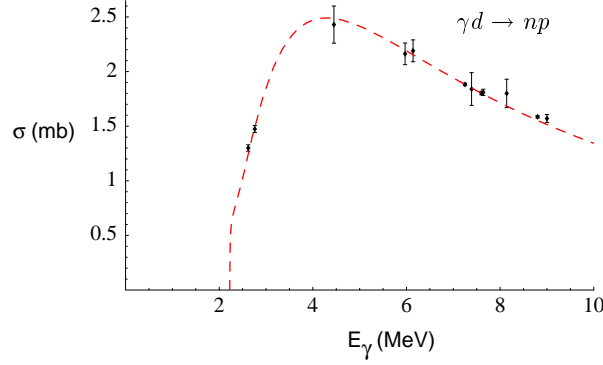


Figure 3: Cross section for $\gamma + d \rightarrow n + p$ as function of the photon energy at N⁴LO, compared to data. From Ref. (31), courtesy of G. Rupak.

interplay of Coulomb interactions were analysed in Ref. (35). These reactions are essential for the understanding of solar neutrino physics since they are relevant for both the production ($p + p \rightarrow d + e^+ + \nu_e$) and detection in heavy water detectors (through the neutral current $\nu + d \rightarrow \nu + n + p$ and the charged current $\bar{\nu} + d \rightarrow e^+ + n + n$ reactions).

The weak interactions are described by the familiar neutral and charged current pieces

$$\mathcal{L} = -\frac{G_F}{\sqrt{2}}(l_{Z\mu}J_Z^\mu + l_{+\mu}J_-^\mu + \text{h.c.}), \quad (26)$$

with the leptonic currents $l_{Z\mu} = \bar{\nu}(1 - \gamma_5)\gamma_\mu\nu$, $l_{+\mu} = \bar{\nu}(1 - \gamma_5)\gamma_\mu e$ and hadronic currents $J_-^\mu = V_-^\mu - A_-^\mu$ and $J_Z^\mu = -2\sin^2\theta_W V_0^\mu + (1 - 2\sin^2\theta_W)V_3^\mu - A_0^\mu - A_3^\mu$. The isosinglet vector (axial) current V_0^μ (A_0^μ) and isotriplet vector (axial) current V_A^μ (A_A^μ), written in terms of the nucleon fields, have contributions in the form of one- and two-nucleon operators. The one-nucleon operators are determined by the axial coupling constant $g_A = 1.26$, the neutron and proton magnetic moments κ_n and κ_p , the strange contribution to the proton spin $\langle \bar{s}\gamma^\mu\gamma_5 s \rangle$ and the strange magnetic moment of the proton μ_s . The two-nucleon currents contributing up to N²LO are

$$\begin{aligned} \mathcal{A}_a^i &= L_{1A}(NP^i N)^\dagger(NP_a N), \\ \mathcal{A}_0^i &= -2iL_{2A}\epsilon_{ijk}(NP^i N)^\dagger(NP^j N) + \text{h.c.}, \\ \mathcal{V}_a^i &= 2iL_1\epsilon_{ijk}(NP^j N)^\dagger(\vec{\nabla}^k + \overleftarrow{\nabla}^k)(NP_a N), \\ \mathcal{V}_0^i &= 2iL_2(NP^j N)^\dagger(\vec{\nabla}_j + \overleftarrow{\nabla}_j)(NP^i N). \end{aligned} \quad (27)$$

$L_1 = L_{M1V}$ was determined through the neutron-proton cold-capture cross section and L_2 was determined by the value of the deuteron magnetic moment. The parameters L_{2A} , $\langle \bar{s}\gamma^\mu\gamma_5 s \rangle$ and μ_s , which are not well determined experimentally, have a negligible impact on the cross section ($< 1\%$) due to the almost orthogonality between initial and final states in the triplet channel. The only relevant unknown in a N²LO calculation is then the value of L_{1A} . Using the estimate in Eq. (15) we find $L_{1A} \sim 4\pi/M\mu^2 \sim 5 \text{ fm}^3$. It is found that two potential-model results, one with and another without exchange-current terms, and differing by about 5%, can be reproduced by varying the value of L_{1A} within this range.

This shows that the difference between these calculations comes from different assumptions about the short-distance physics. To fix this indeterminacy and, consequently, have predictions for the νd reactions at the percent level the value of L_{1A} needs to be determined experimentally. One possibility is the measurement of one of these reactions at one energy. The other is to extract L_{1A} through another process sensitive to this term, like tritium β -decay or muon capture on the deuteron. The challenges involved in this extraction from the well-measured value of the tritium lifetime will be discussed below.

2.2 The three-body system and the limit cycle

The study of three-nucleon systems using EFT is still in its infancy compared to its mature status in the two-nucleon sector. Only now calculations accurate enough are appearing for the triton- ^3He channel that open the door for precision calculations of processes involving external currents. Those processes may turn out to be a very important way of fixing the value of two-body LECs that are hard to measure in the deuteron. The new ingredients in going from two- to three-body systems are three-body interactions. In the absence of fine-tuning their typical size is determined by dimensional analysis. Since they subsume physics contained within the range $1/\Lambda \sim 1/m_\pi$, a three-body force with $2n$ derivatives would have the typical size

$$\mathcal{L}_3 = D_{2n} \bar{\delta}^{2n} (N^\dagger N)^3 \rightarrow D_{2n} \sim \frac{(4\pi)^2}{M\Lambda^{4+2n}}. \quad (28)$$

Just as it happens in the two-body force, the fine-tuning in the two-body S -wave channels introduces a new scale $\gamma \sim 1/a_s$ that invalidates the estimate in Eq. (28). We will resort to the same argument used before to estimate the size of these contributions. We will demand observables to be cutoff independent order by order in the low-energy expansion, which determines the running of the three-body forces with the assumption that their typical size is set by the size of their running, $D_{2n}(\Lambda) \sim D_{2n}(2\Lambda) - D_{2n}(\Lambda)$. As mentioned before, it is unlikely that $D_{2n}(\Lambda)$ is much smaller than this estimate for a particular value of the regulator Λ , or that it contains a large Λ -independent piece. Another way of looking at this way of estimating the LECs is to remember that if the inclusion of a particular LEC is necessary in order to have cutoff-independent results (at a particular order in the expansion), this LEC needs to be large enough to appear at that same order of the expansion.

The doublet S -wave channel (where the triton and ^3He are) has a very different behavior from the other channels. The physical reason is that this is the only channel where all three nucleons can occupy the same point in space (two spin and two isospin states allow for a maximum of four nucleons in the same state). A system of three bosons also displays this property and is qualitatively similar to three nucleons in the doublet S -wave channel. In the remaining channels either the angular-momentum barrier or the Pauli exclusion principle forbids the three nucleons to touch. One would then expect that the doublet S -wave channel (and systems of three bosons) are much more sensitive to short-distance physics than the other channels, an expectation that we will see confirmed by further analysis.

To avoid unnecessary complications we will present explicit expressions only for the case of the S -wave three-boson system. The formulae for the nucleon cases in the different channels can be deduced in an analogous way and can be

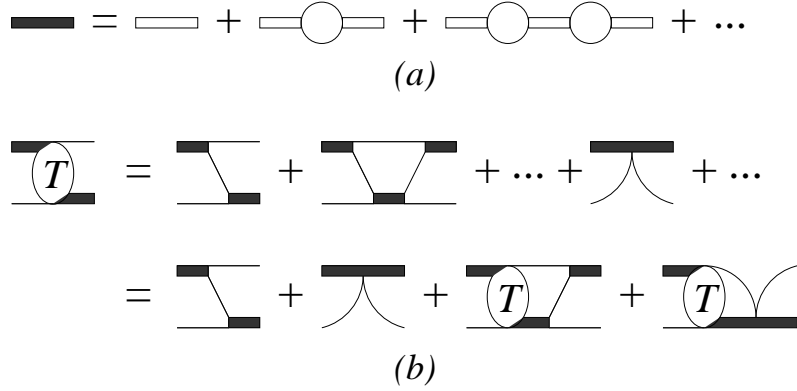


Figure 4: LO graphs contributing to the dressed propagator of the dimeron (a) and to the particle/dimeron amplitude (b).

found, for instance, in Refs. (36,38,37). A convenient first step is to rewrite the action in terms of an auxiliary “dimeron” field d (39),

$$\begin{aligned}
\mathcal{L}_{bosons} &= N^\dagger(i\partial_0 + \frac{\vec{\nabla}^2}{2M} + \dots)N - C_0(NN)^\dagger NN - D_0(NNN)^\dagger NNN + \dots \\
&\rightarrow N^\dagger(i\partial_0 + \frac{\vec{\nabla}^2}{2M} + \dots)N + \Delta d^\dagger d \\
&\quad + y(d^\dagger NN + dN^\dagger N^\dagger) + gd^\dagger dN^\dagger N + \dots,
\end{aligned} \tag{29}$$

where $C_0 = y^2/\Delta$ and $D_0 = -gy^2/\Delta^2$. The equivalence between the two Lagrangians above can be shown by simply performing the Gaussian integral over the auxiliary field d . Since d has the quantum numbers of a two-particle bound state, it can be used as an interpolating field for the bound state. Note that the normalization of the field d (and the value of Δ) is arbitrary and all the observables should be a function only of the combinations y^2/Δ and gy^2/Δ^2 , not of y , g and Δ separately.

The propagator $\Delta(p)$ for the dimeron field of momentum p is given by the sum of bubble graphs shown at the top of Fig. (4). The power counting leading to the necessity of summing all these graphs when the scattering length is large is identical to the one discussed in connection to NN scattering. Taking the arbitrary constant Δ to scale as $\Delta \sim 1$, we have $y^2 \sim C_0 \sim 4\pi/MQ$ and thus $\Delta(\mathbf{p})$ scales as $\Delta(p) \sim (4\pi/MQ)(1/Q) \sim 1$. Summing all graphs, we can write

$$\Delta(p) = \frac{1}{-\gamma + \sqrt{\frac{3p^2}{4} - ME}}. \tag{30}$$

Let us now consider the graphs describing the scattering of one particle off the bound state of other two, shown at the bottom of Fig. (4). We can determine the impact of each graph by power counting. For each additional loop we have two particle propagators, one d propagator, two powers of y and one loop integration, for a total of $(M/Q^2)^2(1)(4\pi/MQ)(Q^5/4\pi M) \sim 1$. There is no suppression for additional loops, and all diagrams involving an arbitrary number of particle exchanges contribute at LO. Graphs including the two-body C_2 operator are suppressed and start appearing at NLO. Graphs including the three-body force may

or may not be leading, depending of the size of the three-body forces. Since at this point we do not know how large they typically are, we will provisionally include them. The chain of diagrams to be summed, contrary to the two-particle case, does not form a simple geometrical series and cannot be summed analytically. We can however consider the second line in Fig. (4) as an equation determining this sum. For the bosonic case, $\lambda = 1$, we have

$$t_k(p) = K(p, k) + \frac{2H}{\Lambda^2} + \frac{2\lambda}{\pi} \int_0^\Lambda dq q^2 \Delta(q) \left(K(p, q) + \frac{2H}{\Lambda^2} \right) t_k(q), \quad (31)$$

with

$$\begin{aligned} K(p, q) &= \frac{1}{pq} \ln \left(\frac{p^2 + pq + q^2 - ME}{p^2 - pq + q^2 - ME} \right), \\ H(\Lambda) &= \frac{g\Lambda^2}{4My^2}, \end{aligned} \quad (32)$$

where $t_k(p)$ is the scattering amplitude with all but the outgoing single-particle line on-shell (“half-off-shell amplitude”), k is the incoming momentum in the center-of-mass system, p is the outgoing momentum, and $E = 3k^4/4m - \gamma^2$ is the total energy. The on-shell point is at $p = k$. In the case of nucleons in the quartet channel the same equation is obtained, but with $\lambda = -1/2$ and some additional momentum dependence in the three-body force (since the simple momentum-independent three-body force does not contribute to this channel). Because all spins are parallel in the quartet channel, only triplet two-body interactions occur and the value of γ is determined by the deuteron pole. The auxiliary field d carries the quantum numbers of the deuteron. In the doublet case, singlet and triplet two-body interactions contribute. The analog of Eq. (31) is a pair of coupled integral equations that, in the $SU(4)$ limit⁷ where the singlet and triplet scattering lengths are equal (or in the ultraviolet where $1/a_s$, γ can be discarded) decouple into a pair of equations like Eq. (31), one with $\lambda = 1$, another with $\lambda = -1/2$. Two auxiliary fields appear, one with the quantum numbers of the deuteron, another with the 1S_0 quantum numbers. In all spin channels, equations for the higher partial waves are obtained by substituting the logarithm in the kernel by a Legendre function $Q_l(pq/(p^2 + q^2 - ME))$. Eq. (31) is the version of the Faddeev equation (see Ref. (41) for a nice introduction) appropriate for contact interactions. It was first derived, by very different methods, in Ref. (42). It is only for *separable* potentials, like the contact interactions considered here, that the Faddeev equation reduces to a one-dimensional integral equation. This simplification reduces the numerical work involved by many orders of magnitude.

2.2.1 Most channels are easy

Let us first consider the channels in the second group, that is, all channels but the doublet S wave. The diagrams summed by Eq. (31) are all ultraviolet finite. That would suggest that there is no need to include three-body forces to absorb the cutoff dependence since this dependence is a subleading $1/\Lambda$ effect. The (numerical) solution confirms this. Even in the absence of a three-body force the phase shifts are only weakly dependent on Λ and $t_k(k)$ has a finite limit when $\Lambda \rightarrow \infty$. Higher-order corrections can be included either perturbatively (as was done

⁷See Ref. (40) for a discussion of the $SU(4)$ limit in the two-nucleon sector.

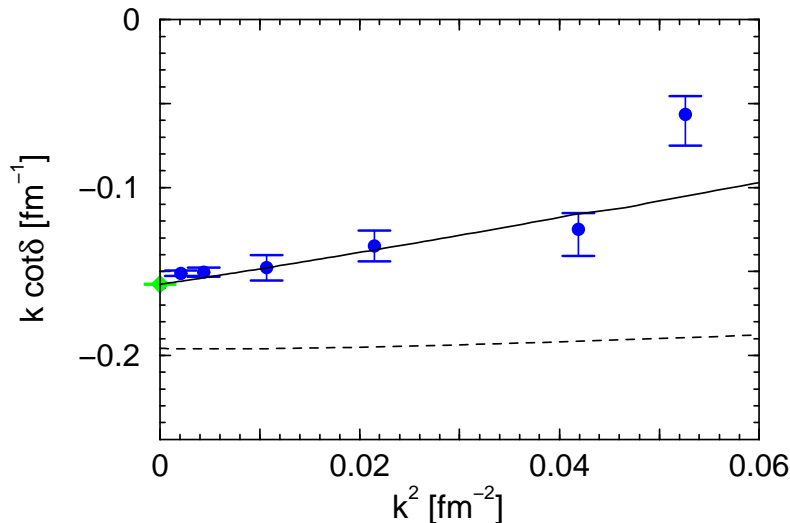


Figure 5: $k \cot \delta$ for nd scattering in the quartet S -wave channel as function of the energy. The dashed line is the LO and the full line the N^2 LO result (36). Points are from a PSA (43) and a near-threshold measurement (44). Figure courtesy of H.-W. Hammer.

in the two-body sector) or non-perturbatively through the denominator in the dimeron propagator. This last resummation amounts to including some (but not all!) higher-order effects. It can be automatically computed by solving a modified version of Eq. (31), which is easier than performing perturbative calculations at high orders. Calculations of the neutron-deuteron (nd) phase shifts are presently available up to N^2 LO (12,36,37). At this order the only inputs are γ and r_{0t} (for the three-body quartet channels), and $1/a_s$ and r_{0s} (needed only for the doublet channels). There are no unknown LECs appearing at N^3 LO, so this approach can be easily pushed to higher orders (and precision). For a flavor of the results, we show the predicted quartet S -wave phase shift in Fig. (5), compared to a PSA (43) (at finite k) and a scattering length measurement (44) (essentially at $k = 0$).

Most of the data is not precise enough to provide a strict test for the convergence of the low-energy expansion, but the zero-energy point is much better measured. The EFT calculation gives for the quartet S -wave scattering length $a_{3/2} = 5.09 + 0.89 + 0.35 + \dots = 6.33 \pm 0.05$ fm (42,45,12), while the experimental value is $a_{3/2}^{exp} = 6.35 \pm 0.02$ fm (44). The EFT error is probably overestimated since the N^2 LO calculation resummed some of the N^3 LO pieces and the remaining ones are known to be smaller than the naive estimate (like the effect of the two-body shape parameter). Since the whole input in these calculations were the threshold parameters of NN scattering, these results are universal (a “low-energy theorem”). Any model with the correct scattering lengths and effective ranges (and not wildly wrong phase shifts above threshold) should reproduce them, within the estimated error. The small discrepancy with “first-generation” NN potentials can be explained by the imprecise values of $a_{s,t}$ that those models predicted. “Second-generation” (or “realistic”) potentials fixed this discrepancy (46).

Coulomb interactions are important in proton-deuteron scattering at small

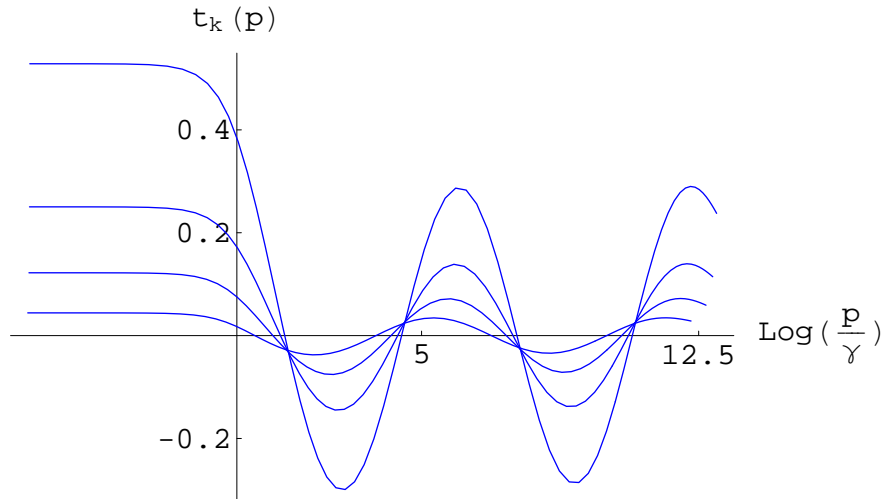


Figure 6: Zero-energy half-off-shell amplitude for boson/two-boson scattering as a function of the outgoing momentum p , from a numerical solution of Eq. (31) with no three-body force, for several different cutoffs.

energies. In Ref. (47) it was shown how they can be easily incorporated in the quartet channels by a simple change in the kernel of Eq. (32).

2.2.2 Triton- ^3He channel and the limit cycle

The change of sign of λ between the bosonic and quartet equations qualitatively changes the behavior of respective solutions. The most striking feature is that the solution of the bosonic (and of the S -wave doublet) equation in the absence of a three-body force depends sensitively on the value of cutoff used. This happens despite the fact that, as mentioned above, there is no ultraviolet divergence in the graphs summed. To illustrate this we show in Fig. (6) the $k = 0$ solutions of Eq. (31) corresponding to various cutoffs (with $\lambda = 1$, $H = 0$). Notice that the three-body scattering length, determined by the asymptotic plateau on the left, $t_{k=0}(k = 0)$, can take any value by just varying the cutoff within a reasonable range.

It has been known for a long time that Eq. (31) is not well defined in the limit $\Lambda \rightarrow \infty$. This disease can be shown in a variety of ways (48, 49, 50, 21). Consider the intermediate-momentum regime $Q \ll p \ll \Lambda$ (remember that Q stands for any infrared scale $Q \sim \gamma \sim k$). Up to terms suppressed by powers of Q/Λ , and assuming $H \sim 1$, Eq. (31) reduces to (48)

$$t_k(p) = \frac{4}{\sqrt{3}\pi} \int_0^\infty dq \frac{1}{q} \ln \left(\frac{p^2 + pq + q^2}{p^2 - pq + q^2} \right) t_k(q). \quad (33)$$

Eq. (33) has two symmetries⁸

$$\begin{aligned} t_k(p) &\rightarrow t_k(\alpha p) \quad (\text{scale invariance}) \\ t_k(p) &\rightarrow t_k(1/p) \quad (\text{inversion symmetry}), \end{aligned} \quad (34)$$

that suggest the power-law solution $t_k(p) \sim p^s$. The allowed values of s are determined by plugging this *ansatz* back into Eq. (33). For values of s such that $\mathbf{Re}(s) < 0$ we find

$$\frac{8\lambda}{\sqrt{3s}} \frac{\sin \frac{\pi s}{6}}{\cos \frac{\pi s}{2}} = 1. \quad (35)$$

For values of λ smaller than $\lambda_c \equiv 3\sqrt{3}/4\pi = 0.4135\dots$, the roots of Eq. (35) have $\mathbf{Re}(s) < -1$ and the half-off-shell amplitude goes rapidly to zero as $p \rightarrow \infty$. In the quartet channel, for instance, $t_k(p) \sim 1/p^{3.17}$, which is a softer ultraviolet behavior than the one expected in perturbation theory, $t_k(p) \sim 1/p^2$. For the S -wave doublet case (or the bosonic case) though, $\lambda = 1$ and there is a pair of imaginary solutions $s = \pm is_0$, with $s_0 = 1.006\dots$. The asymptotic behavior of the half-off-shell amplitude is then

$$t_k(Q \ll p \ll \Lambda) = A \sin(s_0 \ln p + \delta) \quad (36)$$

where A and δ are p -independent numbers. This oscillatory behavior can be seen in Fig. (6).

The normalization A is fixed by the inhomogeneous term in Eq. (31). Because that is important only in the infrared region $p \sim Q$, A can be determined only by matching Eq. (36) to the solution in the infrared region. The phase δ is determined by matching Eq. (36) to the solution in the ultraviolet region and will depend on the ultraviolet physics (like the value of the regulator Λ and the three-body force $H(\Lambda)$). Actually, by dimensional analysis, the Λ dependence of δ has to be the form $\delta(\Lambda) = -s_0 \ln \Lambda + \bar{\delta}$. If Λ is varied while keeping H constant, as we have done so far, the dependence on the asymptotic phase δ will “spill over” the infrared region and change the on-shell amplitude by a factor of $\mathcal{O}(1)$. On the other hand, δ does not depend on the infrared scales (k , γ , $1/a_s$) and so $H(\Lambda)$ can be adjusted in such a way that $\delta = -s_0 \ln \Lambda + \bar{\delta}(H(\Lambda)) \equiv -s_0 \ln \bar{\Lambda}$ is cutoff independent (for any value of k), with $\bar{\Lambda}$ being a constant. Thus, the requirement of cutoff invariance means that $H(\Lambda)$ runs at LO and, for generic values of Λ , $H(\Lambda) \sim 1$. The typical size of the three-body force is then

$$D_0 \sim \frac{(4\pi)^2 H}{M\Lambda^2 Q^2} \sim \frac{(4\pi)^2}{M\Lambda^2 Q^2}, \quad (37)$$

as opposed to the naive estimate in Eq. (28). This means that D_0 is enhanced in the presence of fine-tuning in the two-body sector by a factor of $(\Lambda/\gamma)^2$. The arbitrary parameter $\bar{\Lambda}$ has to be fixed by one piece of experimental input coming from a three-body observable. The two-body phase shifts are *not* enough to fix the three-body physics already at LO. Another way of looking at the renormalization of the three-body system that is more easily generalizable to higher-order calculations is to consider two amplitudes $t_k^\Lambda(p)$ and $t_k^{\Lambda'}(p)$ obtained by solving

⁸These symmetries suggest that in the limit $\gamma, 1/a_s \rightarrow 0$ the full conformal symmetry holds. In the two-body sector it was shown that this is indeed the case, even for off-shell amplitudes (51). It is not known whether the three-body amplitude is conformal in this limit. The three-body forces break scale invariance at the order they first appear.

Eq. (31) with two cutoffs Λ and Λ' and the corresponding three-body forces $H(\Lambda)$ and $H(\Lambda')$. The integral equation determining $t_k^{\Lambda'}(p)$ can be written as

$$\begin{aligned}
 & \int_0^\Lambda dq \left(\delta(p-q) - \frac{2}{\pi} q^2 \Delta(q) K(p,q) \right) t_k^{\Lambda'}(q) \\
 = & K(p,k) + \frac{2H(\Lambda)}{\Lambda^2} + \frac{2}{\pi} \frac{2H(\Lambda)}{\Lambda^2} \int_0^\Lambda dq q^2 \Delta(q) t_k^{\Lambda'}(q) \\
 & + \frac{2H(\Lambda')}{\Lambda'^2} - \frac{2H(\Lambda)}{\Lambda^2} + \frac{2}{\pi} \left(\frac{2H(\Lambda')}{\Lambda'^2} - \frac{2H(\Lambda)}{\Lambda^2} \right) \int_0^\Lambda dq q^2 \Delta(q) t_k^{\Lambda'}(q) \\
 & + \frac{2}{\pi} \int_\Lambda^{\Lambda'} dq q^2 \Delta(q) \left(K(p,q) + \frac{2H(\Lambda)}{\Lambda^2} \right) t_k^{\Lambda'}(q). \tag{38}
 \end{aligned}$$

The first two lines in Eq. (38) are identical to the equation determining $t_k^\Lambda(p)$. If the effect of the remaining terms are small (up to terms of $\mathcal{O}(Q/\Lambda)$), $t_k^\Lambda(p) = t_k^{\Lambda'}(p)$ (again, up to terms of $\mathcal{O}(Q/\Lambda)$). These terms are indeed small, suppressed by a factor of Q/Λ compared to the leading ones. However, their effect on $t_k^\Lambda(p)$ is not suppressed. That is because the operator acting on $t_k^\Lambda(p)$ on the left-hand side of Eq. (38) is nearly singular, that is, it has a small eigenvalue of order Q/Λ .

$$\int_0^\Lambda \left(\delta(p-q) - \frac{2}{\pi} q^2 \Delta(q) K(p,q) \right) a(q) = \mathcal{O}(Q/\Lambda) a(p) \tag{39}$$

The eigenfunction $a(p)$ has the same asymptotics shown in Eq. (36) as $t_k^\Lambda(p)$. In our determination of the asymptotics, Eq. (36), we have already shown Eq. (39) in the limit $\Lambda \rightarrow \infty$ and the total energy $E \rightarrow 0$. We now see that the operator in the left-hand side of Eq. (38) is almost non-invertible and that the projection of $t_k^\Lambda(p)$ in the $a(p)$ direction is sensitive to the $\mathcal{O}(Q/\Lambda)$ terms in the right side of Eq. (38). The amplitudes computed with different Λ 's shown in Fig. (6) indeed differ in the intermediate regime by a term of the form $\sin(s_0 \ln p + \delta)$. The solution $t_k^\Lambda(p)$ has an increased sensitivity to the ultraviolet physics and changes by a factor of $\mathcal{O}(1)$ if the right-hand side of Eq. (38) changes by a factor of $\mathcal{O}(Q/\Lambda)$. That explains the apparent contradiction between the cutoff sensitivity and the absence of ultraviolet divergences.

Using the asymptotic form of $t_k^\Lambda(p)$, Eq. (36), even in the region $p \sim \Lambda$ where it is unjustified, and dropping the terms suppressed by $(Q/\Lambda)^2$ we can derive an approximate analytical expression for $H(\Lambda)$ needed to cancel the Q/Λ terms in Eq. (38) (and to guarantee $t_k^\Lambda(p)$ is cutoff independent up to order Q/Λ):

$$H(\Lambda) = \frac{\cos\left(s_0 \ln \frac{\Lambda}{\bar{\Lambda}} + \arctan s_0\right)}{\cos\left(s_0 \ln \frac{\Lambda}{\bar{\Lambda}} - \arctan s_0\right)}, \tag{40}$$

where $\bar{\Lambda}$ is the parameter determining the asymptotic phase, to be fixed by experiment. We show $H(\Lambda)$ in Fig. (7). The points there were determined by numerically finding values of $H(\Lambda)$ that, when inserted in Eq. (31), reproduce the same three-body phase shifts for different values of Λ . The solid line is Eq. (40). The agreement between Eq. (40) and the numerical points, as well as the independence of the phase shifts with Λ after $H(\Lambda)$ is properly changed, confirms our understanding of this somewhat unusual renormalization. For further discussion of renormalization-group invariance at this order, see Ref (52).

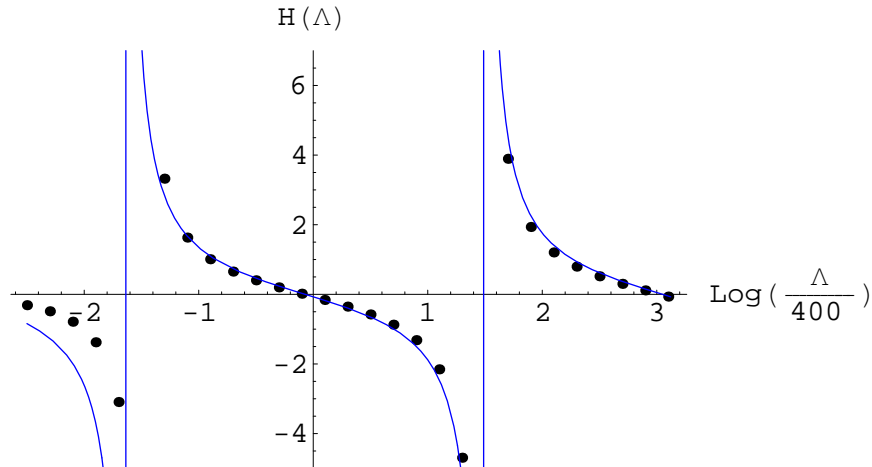


Figure 7: Three-body force coefficient $H(\Lambda)$ computed analytically (blue line) and numerically (black dots) as a function of $\log(\Lambda/400 \text{ MeV})$.

The asymptotic running of the three-body coupling can be interpreted as a limit cycle. The possibility of limit cycles in addition to fixed points was suggested in Ref. (53), but apparently never before seen in a simple physical system. Limit cycles are now being further studied (54).

NLO calculations of phase shifts were performed in Ref. (55) (scattering lengths were computed by different, but equivalent methods in Refs. (49,45)). No new three-body force is needed at this order (although $H(\Lambda)$ has a correction proportional to the two-body effective range). As in other channels, it is easier to compute higher-order corrections by computing the kernel at the order desired and iterating it. That is, one numerically solves Eq. (31) with a kernel that includes higher-order effects. At NLO we demand $t_k^\Lambda(p)$ to be independent of Λ up to terms of $\mathcal{O}(Q/\Lambda)^2$. Due to the almost singular nature of the integral equation, the right-hand side of Eq. (38) has to be Λ independent up to terms of order $(Q/\Lambda)^3$. This can be accomplished with the same no-derivative three-body force because the terms in the right-hand side of Eq. (38) of $\mathcal{O}(Q/\Lambda)^2$ are k, p independent. (However, $H(\Lambda)$ will have a different form than in Eq. (40)). Similarly, at N²LO we need to cancel the $\mathcal{O}(Q/\Lambda)^3$ terms in the right-hand side. Those terms, however, are proportional to k^2, p^2 and can be absorbed only by a three-body force with two derivatives. So, at N²LO, a new three-body force appears, and we need yet another piece of three-body data to fix this new LEC. The cutoff sensitivity is dramatically reduced by going to higher orders, as it should (56). In Fig. (8) we show the phase shifts in the S -wave doublet channel computed at the first three orders (56). As inputs in these calculations we have, besides the two-body interactions, a no-derivative three-body force fitted to the experimental binding energy of the triton at LO and a two-derivative three-body force fitted to the experimental value of the doublet nd scattering length at NLO. The EFT results are compared to a PSA (43) and to results from the Argonne

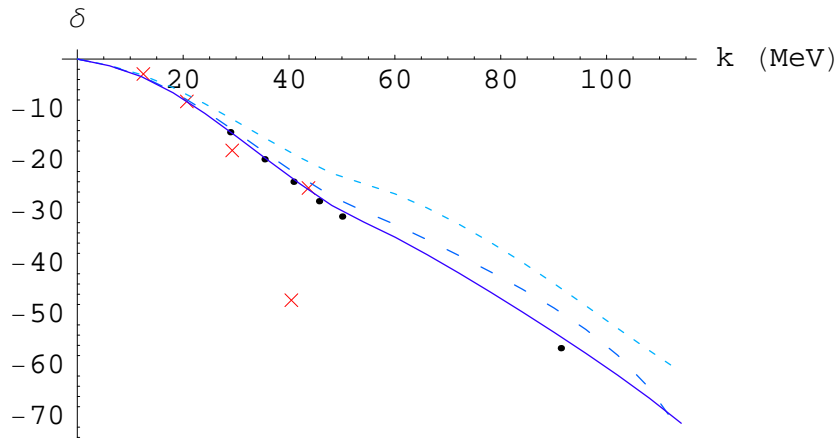


Figure 8: nd phase shift (in degrees) in the doublet S -wave channel as function of the center-of-mass momentum: EFT at LO (light-blue dotted line), at NLO (blue dashed line), and at N²LO (purple solid line), a PSA (red crosses), and a potential model (black dots). From Ref. (56).

V18 potential plus the Urbana three-body force adjusted to reproduce the correct triton binding energy (57).

The existence, already at LO, of a parameter not determined by NN scattering means that models tuned to reproduce the low-energy NN phase shifts may differ widely on their predictions for three-body properties. However, since up to NLO there is only a one-parameter arbitrariness in the three-body predictions, there must be correlations among these predictions. This was noted empirically in Ref. (58). Fig. (9) shows results for the doublet S -wave scattering length and the triton binding energy from a number of models, all reproducing the same low-energy NN scattering (59). The predictions cover a wide range but show a clear correlation (“Phillips line”). Also shown are the LO and NLO predictions for this correlation, obtained by varying the value of the three-body force at fixed cutoff. An equivalent explanation for the existence of the Phillips line was first found in Ref. (60). Analogous results can be obtained in the EFT for the hypertriton (61).

In the $3N$ system, the pionless EFT seems to converge over a range of momenta that is large enough to include the interesting physics associated with the bound states. For example, if the three-body force is fitted to the scattering length, binding energy of triton is $B_3 = 8.08 + 0.23 + \dots = (8.31 + \dots)$ MeV (38,56), to be compared to the experimental result $B_3^{exp} = 8.48$ MeV. The success of these EFT calculations opens the way for the study of low-energy reactions involving triton and ${}^3\text{He}$.

3 EFT WITH EXPLICIT PIONS

As the typical momentum Q approaches the pion mass m_π , it becomes increasingly difficult to account for pion exchange as a short-range effect. As we further

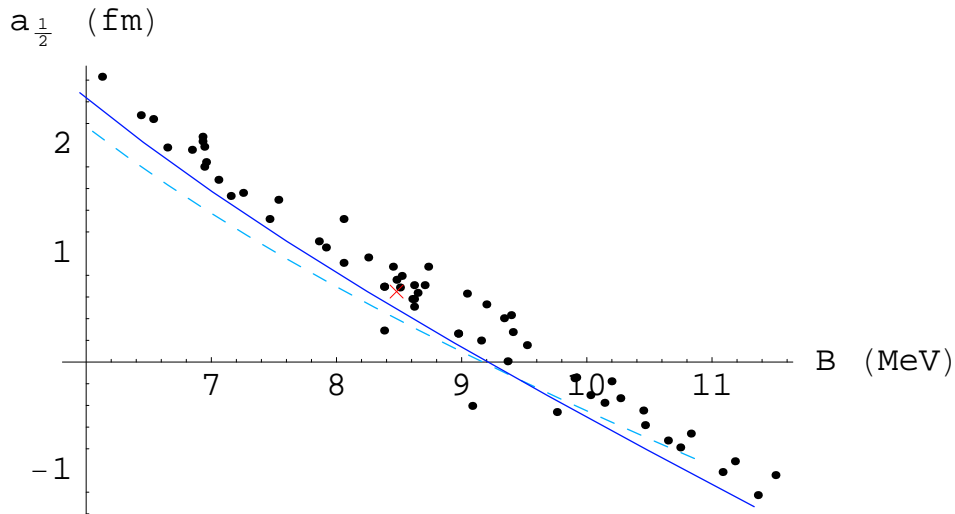


Figure 9: Correlation between the doublet S -wave Nd scattering length and the triton binding energy (Phillips line): predictions of different models (black points), EFT in LO (light dashed line) and NLO (dark solid line), and experimental value (red cross).

increase momenta past $Q \sim m_\pi$, we have to include in the EFT an explicit pion field and build up all its interactions allowed by symmetries. Because *numerically* the mass difference between the delta isobar and the nucleon, $\delta m = m_\Delta - m_N$, is $\sim 2m_\pi$, convergence of the “pionful” EFT is optimized by the concomitant inclusion of an explicit delta degree of freedom. The delta can be included without additional problems, since at these momenta the delta is, like the nucleon, a non-relativistic object. All other degrees of freedom can be considered heavy. Their effects are still subsumed in contact interactions, as they were in the pionless EFT. What we are doing is to remove part of the pion (and possibly the isobar) contributions from the contact interactions. One hopes the new EFT works for momenta up to $M_{QCD} \sim 1$ GeV, the mass scale of the heavier particles.

Adding explicit pions to the theory will generate all sorts of non-analytic contributions to nuclear amplitudes. We want to devise a rationale for a controlled expansion in the presence of pions.

3.1 Chiral symmetry and Chiral Perturbation Theory

Fortunately, pion interactions are not arbitrary. Once explicit pion fields are considered, approximate chiral symmetry imposes important restrictions on the way pions couple among themselves and to other degrees of freedom.

In the limit where we neglect the masses m_u and m_d of the up and down quarks (“chiral limit”), QCD has a chiral $SU(2)_L \times SU(2)_R$ symmetry. Since this symmetry is not apparent in the QCD spectrum, it is reasonable to assume that it is broken spontaneously down to its diagonal subgroup, the $SU(2)_{L+R}$ of isospin. Goldstone’s theorem (62) tells us that massless Goldstone bosons, naturally identified as pions, are associated with the three broken generators,

and their fields $\boldsymbol{\pi}$ live on the “chiral circle” (actually a three-sphere S^3) that represents the set of possible vacua. We call the radius of this sphere f_π ; it is directly related to the chiral-symmetry-breaking scale, $\Lambda_{\chi SB} \sim 4\pi f_\pi \sim M_{QCD}$, but the precise factor can only be obtained from the (so far elusive) mechanism of dynamical symmetry breaking in QCD. It turns out that this diameter can be determined from pion decay, and is called the pion decay constant, $f_\pi \simeq 92.6$ MeV.

The “chiral circle” can be parameterized in different ways but it is convenient to choose fields for which chiral symmetry is respected term-by-term in the effective Lagrangian. Since the interactions of pions have to be invariant under chiral rotations, it is possible to choose fields where an infinitesimal rotation is represented as $\boldsymbol{\pi} \rightarrow \boldsymbol{\pi} + \boldsymbol{\epsilon}$. Interactions of these fields always involve derivatives on the sphere, that is, derivatives together with certain non-linear self-interactions.

As long as quark masses are small enough, their only effect is to change this picture slightly. A common quark mass breaks chiral symmetry explicitly down to the diagonal subgroup. Points on the chiral circle are no longer degenerate in energy, and a particular minimum is selected, in a direction given by the quark-mass terms that we define as the fourth direction. The quark mass difference further breaks isospin explicitly. In the low-energy EFT, the effect of quark-mass terms can be reproduced if we construct all terms that break chiral symmetry in the same way. These interactions can involve $\boldsymbol{\pi}$ without derivatives, but are always accompanied by powers of $m_u + m_d$ or $m_u - m_d$. One example is a pion mass term, $m_\pi^2 \propto (m_u + m_d)$. Likewise, electromagnetic and weak interactions can be constructed as well.

The well-studied theory of non-linear representations of symmetries (63) provides the tools to write down the appropriate interactions between pions and other fields. The resulting chiral Lagrangian \mathcal{L} has an infinite number of terms that can be grouped according to the index Δ :

$$\mathcal{L} = \sum_{\Delta=0}^{\infty} \mathcal{L}^{(\Delta)}, \quad \Delta \equiv d + f/2 - 2, \quad (41)$$

where d is the number of derivatives, powers of m_π and/or powers of δm , and f is the number of fermion fields. Because of chiral symmetry, pion interactions stemming from QCD bring derivatives and/or powers of the pion mass. As a consequence, $\Delta \geq 0$. The explicit form of $\mathcal{L}^{(\Delta)}$ for the lower values of Δ can be found in the literature (64, 18).

As in the pionless EFT, the only hope of any predictive power rests on finding some ordering of contributions to amplitudes. This can be done for processes where all the external three-momenta are $Q \sim m_\pi$. Powers of Q of any particular Feynman diagram can be counted as done for the superficial degree of divergence. Each space derivative in an interaction produces a three-momentum in a vertex and therefore counts as Q . A complication in the counting of energies stems from the presence of heavy particles such as the nucleon together with light particles such as the pion. In any loop, integration over the zeroth component of the four-momentum will involve *two* types of poles, according to the scales appearing in the propagators: (i) standard poles at $\sim Q$ corresponding to external three-momenta and to the mass of the pion; and (ii) shallow poles at $\sim Q^2/2m_N$ corresponding to external nucleon energies.

Processes that involve at most one heavy particle ($A = 0, 1$) are the simplest because the contour of integration can always be closed so as to avoid shallow

poles. In this case all energies are $\sim Q$. As a consequence, each time derivative counts as Q and four-momentum integration brings a factor Q^4 . A pion propagator is Q^{-2} and a nucleon (or delta) propagator is Q^{-1} from its static term; kinetic terms are of relative $\mathcal{O}(Q/m_N)$ and thus can be treated as corrections. With these ingredients one can write the contribution of any diagram to the amplitude as

$$T \propto Q^\nu \mathcal{F}(Q/\Lambda), \quad (42)$$

where Λ is a renormalization scale, \mathcal{F} is a calculable function of LECs, and ν is a counting index. For strong interactions (65),

$$\nu = 4 - 2C - A + 2L + \sum_i \Delta_i, \quad (43)$$

where $C = 1$ is the number of connected pieces, L is the number of loops, and the sum runs over all vertices. In addition, electroweak interactions can be considered through a simultaneous expansion in $\alpha = e^2/4\pi$ and $G_F f_\pi^2$. Since $L \geq 0$ and $\Delta \geq 0$, $\nu \geq 2 - A \equiv \nu_{min}$. Assuming that all LECs have “natural” size (given by powers of M_{QCD} once the lower scales have been identified explicitly), an expansion in Q/M_{QCD} results. Its first two orders are equivalent to the current algebra of the 60’s, but at higher orders unitarity corrections can be accounted for systematically. In the sector of $A = 0, 1$, the EFT is called Chiral Perturbation Theory (ChPT).

In processes that involve more than one stable heavy particle ($A \geq 2$), on the other hand, a failure of perturbation theory can lead to bound states (6). The shallow poles cannot be avoided: they represent “reducible” intermediate states that, as in the pionless EFT, differ from initial states only by nucleon kinetic energies, which are $\sim Q^2/m_N$. This $\mathcal{O}(m_N/Q)$ infrared enhancement over intermediate states where energies are $\sim Q$ invalidates Eq. (43) for reducible diagrams. Fermion lines, loops and derivatives then scale with Q as in Eq. (16). A pion propagator still counts as Q^{-2} , but the pion can be taken in first approximation as static, and it is sometimes referred to as a “potential” pion. Contributions that come from standard poles naively scale as in processes with no more than one heavy particle. Pions there are non-static or “radiative”.

The issue now is how to estimate the size of pion contributions. One needs to find the importance of (i) pion exchange relative to short-range interactions; (ii) multi-pion exchange relative to one-pion exchange (OPE). Both issues are related, via renormalization, to the size of the contact interactions. How large are they in the pionful EFT? What are the contributions that *must* be resummed in nuclear amplitudes?

3.2 The two-nucleon system

As we have discussed, the NN system is characterized by scattering lengths a_s , a_t that are much larger than $1/M_{QCD}$. In the pionless theory, this fine-tuning cannot be explained, but it can be accommodated in the power counting by assigning to the contact interactions the scaling given in Eq. (16).

A new scale appears naturally in the pionful theory. The leading ($\Delta = 0$) coupling of the pion to the nucleon is derivative with a coupling constant g_A/f_π , where $g_A \simeq 1.26$ is a parameter not fixed by symmetry but determined in β -decay. The OPE contribution to the NN amplitude is, schematically, $g_A^2 Q^2/f_\pi^2(Q^2 + m_\pi^2)$.

Because a reducible intermediate state contributes $m_N Q/4\pi$, relative to OPE, once-iterated OPE can be estimated to give a contribution

$$\frac{(g_A^2 Q^2/f_\pi^2(Q^2 + m_\pi^2))^2(m_N Q/4\pi)}{g_A^2 Q^2/f_\pi^2(Q^2 + m_\pi^2)} \sim \frac{Q}{M_{NN}} \quad (44)$$

(as long as $Q \gtrsim m_\pi$). Here we introduced the scale

$$M_{NN} \equiv \frac{4\pi f_\pi^2}{g_A^2 m_N}, \quad (45)$$

which sets the relative strength of multi-pion exchange. Numerically (for $N_c = 3$) $m_N \sim 4\pi f_\pi$ and $g_A \sim 1$, so $M_{NN} \sim f_\pi$. This naive dimensional analysis cannot, however, capture the numerical factors that actually set the relative size of pion contributions. A more accurate estimate requires concrete calculations.

3.2.1 Perturbative pions

For $Q \lesssim M_{NN}$, iteration of OPE should be suppressed with respect to OPE according to Eq. (44). Moreover, if we assume that the leading short-range effects are $\sim 4\pi a/m_N$ (as in Eq. (16) with $Q \rightarrow 1/a$), then OPE is suppressed by $\mathcal{O}(1/aM_{NN})$ compared to the leading contact interaction. With such estimates, if M_{NN} is sufficiently large (compared to $1/a$ and m_π) and Q sufficiently small, pions may be treated perturbatively. The suggestion that this can be profitably done was made in Refs. (66, 23).

A simple power counting, which became known as KSW counting, follows by taking $Q \sim 1/a \sim m_\pi < M_{NN}$, and counting powers of the light scale Q . This is a direct extension of the power counting in Eq. (16). In particular, the scaling of the contact operators is assumed to be the same as before with $\Lambda \rightarrow M_{NN}$, and thus their ordering is unchanged. Because of chiral symmetry, each insertion of a pion exchange brings a factor of Q/M_{NN} . Electroweak interactions can be treated in much the same way as before. One can show that renormalization can be carried out consistently within this power counting (23).

However, for this power counting to be relevant to nuclear physics M_{NN} has to be sufficiently large. If M_{NN} is not larger than m_π , the domain of perturbative pions is no larger than that of the simpler pionless theory. The issue of the range of validity of the EFT with perturbative pions can only be settled by explicit calculation of dimensionless factors and comparison with precise observed quantities, this being done to sufficiently high order so that a significant number of pion effects be tested.

With this power counting, the LO NN amplitude coincides with that in the pionless EFT, see Fig. (1). At this order there are contributions only in the two S -wave channels from chirally-symmetric, non-derivative contact interactions (the C_0 terms). Subleading terms, of $\mathcal{O}(Q/M_{NN})$ relative to leading, are constructed in a direct extension of subleading terms of the pionless EFT. Besides two two-derivative contact interactions (C_2 terms), we also insert OPE and two non-derivative contact interactions that break chiral symmetry explicitly ($m_\pi^2 C_2^{qm}$ terms). Both C_2 and C_2^{qm} contact interactions only contribute to S waves. The tensor operator from OPE, on the other hand, introduces mixing between 3S_1 and 3D_1 waves. To this order, all but the S -wave phases are *predicted* in terms of pion parameters. A calculation of the NN system to NLO was carried out in

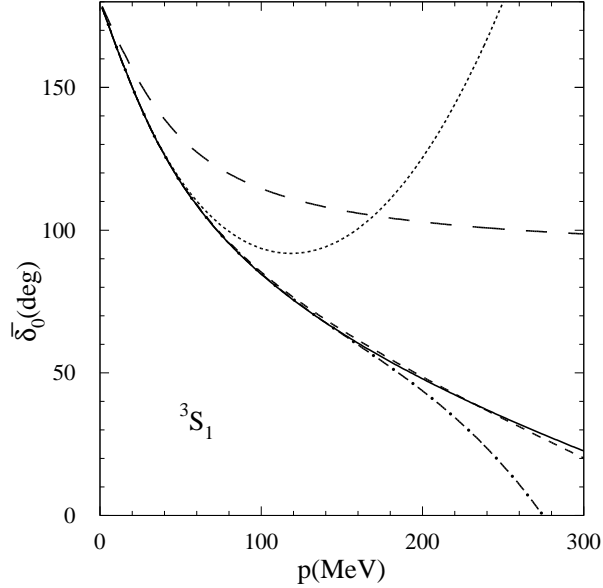


Figure 10: 3S_1 NN phase shift in the EFT with perturbative pions, as function of the center-of-mass momentum. The long-dashed, short-dashed, and dotted lines are, respectively, the EFT results in LO, NLO, and N²LO. The dash-dotted line is the N²LO result with a higher-order contact interaction added. The solid line is the Nijmegen PSA. From Ref. (72), courtesy of T. Mehen.

Refs. (23, 67). When the results were compared to the Nijmegen PSA (26), it was suggested that $M_{NN} \simeq 300$ MeV (23). The relative size of OPE and contact interactions was extensively discussed (68, 69, 70), but the issue is clouded by the details of fitting procedures.

At N²LO we encounter new pion exchanges: both non-static (or radiative) OPE and once-iterated OPE. A calculation at this order was carried out in all S , P , and D waves (72, 71). Results were found to depend on the channel. While in singlet channels, like 1S_0 , there seems to be good agreement with the Nijmegen PSA, in triplet channels, such as 3S_1 , 3D_1 , and ${}^3P_{0,2}$, the N²LO corrections are big at momenta ~ 100 MeV and lead to large disagreement. One example is shown in Fig. (10). The effects of perturbative pions (and of delta isobars) is milder in the higher partial waves (73).

The problem can be traced to the iteration of the tensor part of OPE. These results suggest that pions, or more explicitly, the Yukawa part of potential and radiation pions, when treated perturbatively give rise to a converging expansion for the 1S_0 scattering amplitude up to fairly large momenta. However, OPE in the ${}^3S_1 - {}^3D_1$ coupled channels is *not* perturbatively convergent for momenta around 100 MeV, because the tensor force, which survives in the chiral limit, is too large. This, in turn, suggests that the naive estimate $M_{NN} \sim f_\pi$ is not entirely unreasonable.

3.2.2 Renormalization of the pion ladder and power counting

If indeed $M_{NN} \ll M_{QCD}$, we might hope to improve on the expansion of the previous section by a controlled resummation of terms that go as Q/M_{NN} . If $M_{NN} \sim 100$ MeV, the lack of other known particle thresholds there suggests that the resummation could involve *only* pions. Indeed, Weinberg, who first attempted the use of EFT in the derivation of nuclear forces (6), had already suggested a power counting in which pions appear in leading order, and should therefore be iterated. (Some elements of this power counting had been anticipated by Friar (74)).

Weinberg's original proposal (6) for an EFT describing multi-nucleon systems was to split the full amplitudes into reducible and irreducible parts. Irreducible diagrams, in which typical energies superficially resemble those in ordinary ChPT, should satisfy the power counting, Eq. (43). We call the sum of irreducible diagrams the potential V . Note that the potential, being a set of subgraphs, can be defined in alternative ways. All definitions that exclude the infrared-enhanced contributions but differ by a smaller amount are equally good, as long as no double-counting or omissions are made. A field redefinition might change the potential but not the full amplitude. The important point is that the only scale appearing explicitly in the potential is Q , so that the power counting proceeds as in the case of diagrams with at most one heavy particle. Reducible diagrams can be obtained by sewing together irreducible diagrams via intermediate states that contains the propagation of only the initial particles. The full amplitude T for an A -nucleon system is thus a sum of the potential and its iterations; schematically,

$$T = V + VG_0V + VG_0VG_0V + \dots = V + VG_0T, \quad (46)$$

where G_0 is the A -nucleon free (Schrödinger) Green's function. This is just the Lippmann-Schwinger equation, which is *formally* equivalent to the Schrödinger equation with the potential V , from which wave-functions $|\psi\rangle$ can be constructed.

Unfortunately, just counting powers of Q is not in itself sufficient for an ordering of interactions. We need to find which other scales accompany Q . Given that we do not yet possess a full solution of QCD, it is obvious that some assumptions have to be made about the LECs. Because OPE has short-range components, it is natural to assume that they set the scale for the short-range interactions. In this case, since OPE is $\mathcal{O}(g_A^2/f_\pi^2)$ for $Q \sim m_\pi$, we expect the leading two-nucleon contact interactions to be $\mathcal{O}(4\pi/m_N M_{NN})$. This assumption naturally explains why nuclear bound states are much shallower than naively expected (6,9). The series in Eq. (46) is roughly

$$T \sim \frac{4\pi}{m_N M_{NN}} \left[1 + \mathcal{O}\left(\frac{Q}{M_{NN}}\right) + \dots \right], \quad (47)$$

which requires resummation and exhibits a (real or virtual) bound state at $Q \sim M_{NN}$. In other words, the natural scales for the NN scattering length and for the binding energy of a nucleus are

$$|a| \sim \frac{1}{M_{NN}}, \quad B \sim \frac{M_{NN}^2}{m_N}, \quad (48)$$

respectively. If we use again that $m_N \sim 4\pi f_\pi$ and $g_A \sim 1$, then $B \sim f_\pi/4\pi \sim 10$ MeV. So we find that it is not M_{QCD} by itself that sets the scale for binding

energies, but a certain ratio of powers of f_π and m_N . Now, as we have seen, this is not the whole story. It remains mysterious why the NN (real and virtual) bound states are even shallower, or equivalently, why $|a| > 1/M_{NN}$, by factors of a few. This still has to be accommodated by fine-tuning the contact interactions.

Because they serve as counterterms to pion loops in the potential, which are expected to be suppressed (as in ChPT) by powers of $Q/4\pi f_\pi$, Weinberg implicitly assumed that LECs related to more derivatives and powers of the pion mass contain inverse powers of M_{QCD} . That is, a (renormalized) contact operator with index Δ would scale as

$$C_\Delta \sim \frac{4\pi}{m_N M_{NN} M_{QCD}^\Delta}, \quad (49)$$

as in naive dimensional analysis.

With this assumption and disregarding the fine-tuning, a simple power counting results from taking $Q \sim M_{NN} \sim 1/a \sim m_\pi$. The potential obeys Eqs. (42,43). The leading potential consists of no-derivative, chirally-symmetric contact interactions plus static OPE,

$$V^{(0)} = C_0^{(S)} + C_0^{(T)} \vec{\sigma}_1 \cdot \vec{\sigma}_2 - \left(\frac{g_A}{f_\pi}\right)^2 \mathbf{t}_1 \cdot \mathbf{t}_2 \frac{\vec{\sigma}_1 \cdot \vec{q} \vec{\sigma}_2 \cdot \vec{q}}{\vec{q}^2 + m_\pi^2}, \quad (50)$$

where $\vec{\sigma}_i$ ($2\mathbf{t}_i$) are the Pauli matrices in spin (isospin) space and \vec{q} is the momentum transferred. All contributions to nuclear forces other than Eq. (50) would come as corrections in powers of Q/M_{QCD} , starting at $(Q/M_{QCD})^2$. The structure of the potential rapidly becomes more complex with increasing order (7). The leading potential has to be resummed, while corrections can be treated in perturbation theory. If the corrections are truly small, resumming them should cause no major harm. This method requires numerical solution of the Schrödinger equation and is similar in spirit to the traditional potential-model approach. As we will see below, Weinberg's power counting has been extensively and successfully developed during the past decade to study processes involving few-nucleon systems.

However, there is a subtlety not present in ChPT. Loops in reducible diagrams probe, as other loops do, high energies (when nucleons are far off shell). As in the pionless EFT, the potential does not vanish at large momenta: it is singular. In addition to the delta function and its derivatives already present in the pionless theory, pion exchange generates potentials that behave as $1/r^n$ with $n \geq 3$, as the radial coordinate $r \rightarrow 0$. The large-momentum or short-distance behavior is the same as in the chiral limit $m_\pi^2 \rightarrow 0$. Already in leading order the tensor force goes as $1/r^3$ in the chiral limit. As a consequence of ultraviolet divergences generated by the iteration of the potential, the infrared enhancement of M_{QCD}/M_{NN} might contaminate LECs, possibly invalidating Eq. (49).

The crucial issue is whether, at any given order, all divergences generated by iteration can be absorbed in the parameters of the potential truncated at that order. There is some indication that equally good fits can be achieved in leading orders with various cutoffs (9,75,76,70,77,78), as required of a sensible EFT, but the numerical nature of the results makes a definite answer difficult.

Unfortunately, there seem to be formal inconsistencies in Weinberg's counting (23,69). Divergences that arise in the iteration of leading-order interactions apparently cannot be absorbed by the leading-order operators themselves. Two examples are two-loop diagrams where: *i*) OPE happens between two contact

interactions, having a divergence proportional to the square of the pion mass (23); *ii*) OPE is iterated three times, having a divergence proportional to the square of the momentum (69). Although these two particular cases could be resolved by the promotion to leading order of two counterterms, it is likely that a similar problem would show up at higher orders in the expansion. The correspondence between divergences and counterterms appears to be lost, a fundamental problem with the chiral expansion *and* the momentum expansion resulting from Weinberg power counting.

This argument is not decisive, though. It has been known that in the context of the Schrödinger equation perturbative arguments are not in general reliable for singular potentials (79). The perturbative expansion might have a cut starting at $g_A^2/f_\pi^2 = 0$; insistence on a g_A^2/f_π^2 expansion would then reflect itself on different orders offering correlated contributions to counterterms, each bringing powers of M_{QCD}/M_{NN} yet resulting in a much better behaved sum. How can the resummation be consistent? There is a mapping between the singular two-body $1/r^2$ central potential and the three-body problem with short-range interactions. In Sect. 2.2.2 we saw that for the latter, the renormalization of the nonperturbative equation is very different from the renormalization of individual terms in the associated perturbative series (21). In particular, the relevant counterterm exhibits a limit-cycle behavior.

It turns out that the correct renormalization of singular potentials is, indeed, in general intrinsically nonperturbative (79,80). In contrast to regular potentials, both solutions of the Schrödinger equation for an attractive $1/r^n$ central potential are equally acceptable: the radial wave-function $u(r)$, whose large-distance behavior determines low-energy observables, oscillates rapidly as r decreases. Perturbative approximations to the wave-function fail at distances comparable to the intrinsic scale r_0 present in the potential, as illustrated in Fig. (11). The problem can be rendered essentially cutoff independent with a single counterterm associated with the short-distance physics. For example, short-distance physics can be represented by a square well potential of radius $R \ll r_0$ whose depth $V_0 = V_0(R)$ can be adjusted so that physics at $r \gtrsim r_0$ be independent of R (80). (The advantage of this coordinate-space regulator is that one can do an analytic matching of the outer and inner solutions of the Schrödinger equation, thus finding the desired $V_0(R)$. For another technique to deal with a singular potential, see, for example, Ref. (81).) While for a repulsive potential there exist only fixed points (82), the situation in the attractive case is similar to the three-body system.

These results were extended to the NN potential in the 1S_0 and $^3S_1 - ^3D_1$ channels in Ref. (83), where the long-range part of the potential was taken as that of OPE for $r > R$. The asymptotic behavior is that of the chiral limit, where the relevant scale is $r_0 \sim 1/M_{NN}$. The depths of the short-range part of the potential can be different in the singlet and triplet channels, as there are two parameters ($C_0^{(S)}$ and $C_0^{(T)}$) in Eq. (50).

In the 1S_0 channel the calculation is straightforward. The pion potential is simply a Yukawa, and the explicit solution is

$$V_0(R; n) = -(2n + 1)^2 \frac{\pi^2}{4m_N R^2} - \frac{g_A^2 m_\pi^2}{8\pi f_\pi^2 R} \log \left(\frac{R}{R_*} \right) + \mathcal{O}(R^0), \quad (51)$$

where R_* is an intrinsic length scale to be determined numerically from a fit to low-energy data, and n labels the branch of a cotangent. In the left panel of Fig.

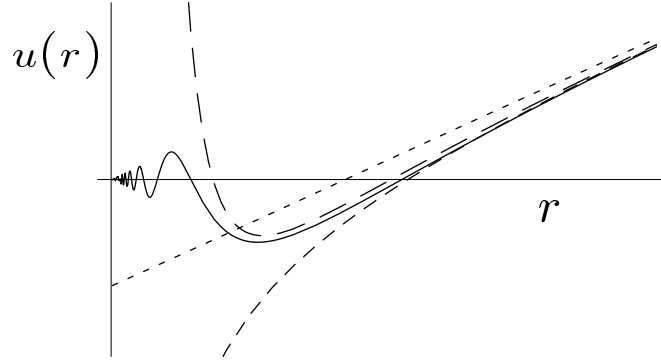


Figure 11: Zero-energy radial wave-functions of the $1/r^4$ potential: exact (solid line) and perturbation theory to LO (small dashes), NLO (medium dashes), and N²LO (large dashes). From Ref. (80).

(12) the R dependence of V_0 , as given by Eq. (51), is compared to the numerical solution of the Schrödinger equation with the observed singlet scattering length. The presence of a multi-branch structure is related to the accumulation of bound states inside the square well. Of course the presence of unphysical bound states is innocuous as long as the binding energies of such states are near the cutoff of the EFT. One sees that the formal problem with the chiral expansion in Weinberg's counting survives the resummation. While the first cutoff-dependent term in Eq. (51) can be represented by a chiral-symmetric contact interaction, the second would require a chiral-breaking one. In momentum-space notation where the cutoff is denoted by Λ ,

$$C_0(\Lambda) + m_\pi^2 C_2^{(qm)}(\Lambda) = \frac{4\pi}{6m_N\Lambda} \left[(2n+1)^2 \frac{\pi^2}{2} + \frac{m_\pi^2}{M_{NN}\Lambda} \log\left(\frac{\Lambda_*}{\Lambda}\right) \right]. \quad (52)$$

Although the logarithmic divergence is suppressed by a power of Λ compared to the first term, it is a true divergence in physical quantities that must be renormalized at leading order in Weinberg power counting. The $C_2^{(qm)}$ operator, which is formally subleading, must be promoted to leading order if the full OPE is iterated, in agreement with the perturbative argument of Ref. (23). On the other hand, the $C_2^{(qm)}$ contribution is numerically small, as demonstrated by the dotted curve in the left panel of Fig. (12) which neglects the Λ^{-2} corrections to the running. This smallness explains why Weinberg's power counting has been found to work well in this channel over a moderate range of cutoffs (9, 75, 76, 77, 70, 78).

A possible conclusion is that OPE and the $\mathcal{O}(m_q)$ LECs contribute to any amplitude at the same order in the expansion, and this is what leads to KSW power counting. However, a more general conclusion to draw is that the difference between the OPE contribution for $m_q \neq 0$ and the OPE contribution in the chiral limit must occur at the same order as the $\mathcal{O}(m_q)$ counterterms. In many cases these two conclusions yield identical amplitudes, however, in the ${}^3S_1 - {}^3D_1$ channel they do not.

In the ${}^3S_1 - {}^3D_1$ channel, in addition to the long-distance Yukawa interaction and the contact interaction, there is a strong tensor component of OPE that cou-

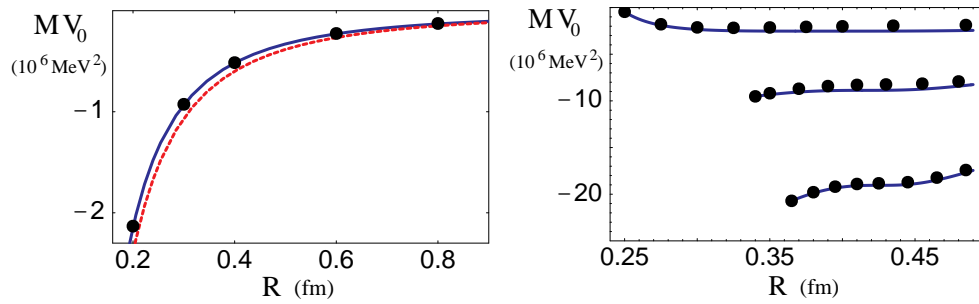


Figure 12: Running of $m_N V_0$ as a function of the cutoff R . Singlet channel (left panel): Eq. (51) for $n = 1$ (blue solid line), and same but with R^{-1} part neglected (red dotted line). Triplet channel (right panel): numerical solution of an analytic matching equation (solid lines). Dots are extracted directly from a numerical solution of the Schrödinger equation in the respective channel. From Ref. (83).

ples S and D waves. At distances $r \ll 1/m_\pi$ the central potential is negligible, while in the region $R < r \ll 1/M_{NN}$ we can neglect the angular-momentum barrier. Moreover, for $\sqrt{m_N E} \ll M_{NN}$ the total energy E can be treated as a perturbation. In this short-distance limit, we can keep only the chiral limit of the tensor force, and the Schrödinger equation can be diagonalized and solved exactly. In the diagonal basis the Schrödinger equation decouples into an attractive singular potential and a repulsive potential. The solution for the attractive singular potential is a linear combination of Bessel functions (84, 80), and the wave-function at this order is

$$u(r) = A r^{3/4} \cos \left(\sqrt{\frac{6}{M_{NN} r}} + \phi_0 \right), \quad (53)$$

where A is a dimensionful normalization constant and ϕ_0 is the asymptotic phase which determines the triplet scattering length. This solution oscillates ever faster as it approaches the origin, just as in Fig. (11). As before, the issue is whether a $V_0(R)$ can be found in such a way that the asymptotic phase ϕ_0 is made R independent. Matching logarithmic derivatives of the interior square-well and exterior attractive solutions at $r = R$ yields an equation whose solution is shown in the right panel of Fig. (12). The renormalization-group flow is multibranched and non-analytic in g_A^2/f_π^2 .

The leading-order 3S_1 phase shift is clearly cutoff independent as shown in Fig. (13). The situation is similar for the 3D_1 phase shift, while the mixing parameter ε_1 exhibits some R dependence. However, an error plot of ε_1 suggests that the R dependence and the deviations from the Nijmegen PSA (26) are higher order in the momentum expansion. These results (83) are in agreement with the numerical analyses of Refs. (84, 77). In these channels, contrary to the perturbative argument (69), Weinberg's power counting does not seem to be formally inconsistent.

It was conjectured in Ref. (83) that a formally consistent expansion in the pionful EFT is an expansion around the chiral limit. This expansion is equivalent

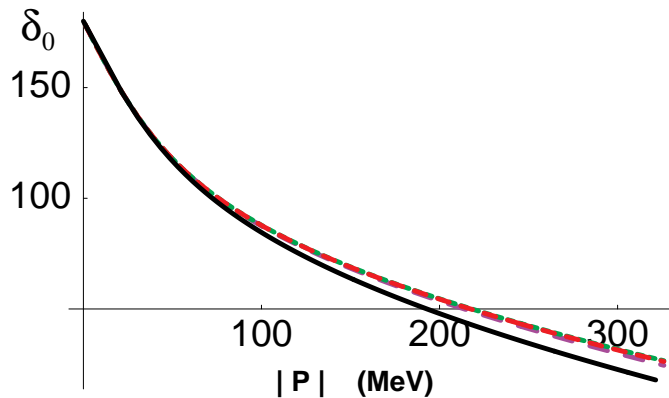


Figure 13: 3S_1 NN phase shift in leading order in the EFT with non-perturbative pions, as function of the center-of-mass momentum. The (purple) long-dashed, (red) medium-dashed, and (red) short-dashed lines have, respectively, $R = 0.45$ fm ($\Lambda = 438$ MeV), $R = 0.21$ fm ($\Lambda = 938$ MeV), and $R = 0.10$ fm ($\Lambda = 1970$ MeV). The (black) solid line is the Nijmegen PSA. From Ref. (83).

to KSW power counting in the 1S_0 channel and equivalent to Weinberg power counting in the ${}^3S_1 - {}^3D_1$ coupled channels, *i.e.* it selects only the desirable features of both power countings. The leading-order potential $V(r;0)$, to be treated exactly, consists of the chirally-symmetric component of OPE and non-derivative contact interactions. Deviations from the chiral limit $V(r; m_\pi) - V(r; 0)$ can be treated perturbatively in all channels, and in fact, such a perturbative expansion is required in the 1S_0 channel but not in the ${}^3S_1 - {}^3D_1$ channel. Evidence was presented that this expansion converges, even though convergence is slow due not to the long-range pion physics itself, but to the fine-tuned short-distance physics (as argued previously (85)).

Although existing obstacles to a derivative and pion-mass expansion were removed, higher orders must be studied before the issue can be considered settled. For example, in Ref. (86) an incomplete sub-leading calculation with non-perturbative pions has found limits in fitting the effective range. Note also that alternative views of the renormalization of the pion ladder exist (87). Finally, there is an interesting suggestion of expanding the NN amplitude in the energy region where the S -wave phase shifts vanish (88). The connection between this expansion and the low-energy expansion described here has not been fully analyzed.

3.2.3 Potentials and fits to NN data

The picture that emerges from the previous section is close, conceptually and numerically, to Weinberg's original proposal. To be formally consistent, we should expand in the pion mass. Yet, if we resum the effects of the pion mass in pion exchange, which can be done with higher-order error, the leading-order potential becomes the same as in Weinberg's power counting. Corrections to the leading potential do not need to be iterated to all orders. Yet, as has been shown explicitly

in the pionless EFT (14), they *can* be iterated with small error, as long as one uses a regularization with a cutoff $\Lambda \sim M_{QCD}$. Clearly, a potential which is correct up to a certain order ensures that the amplitude is correct to the same order.

Much work has been done in developing an EFT potential based on Weinberg's power counting. Traditionally, potential models have been plagued by problems of principle, such as the form of meson-nucleon interactions (for example pseudoscalar *vs.* pseudovector pion coupling), renormalization issues, absence of a small expansion parameter, *etc.* Because the EFT potential includes explicitly the exchange of only pions, all these problems can be resolved. For any given choice of pion field, the form of interactions is fixed by the pattern of chiral symmetry breaking. Renormalization can be performed because *all* interactions consistent with symmetries are included. And the power counting Eq. (43) for the EFT potential implies that diagrams with an increasing number of loops L —and, in particular, with increasing number of exchanged pions—should be progressively less important. The EFT potential can be thought of as a low-energy approximation to standard potential models, although this can only be taken in an average sense.

In leading order, $\nu = \nu_{min} = 0$, the NN potential is, as we saw in the previous section, simply static OPE and momentum-independent contact terms. This is obviously a very crude approximation to the NN potential: it is known that the nuclear force has other sizable components, like a spin-orbit force, a strong short-range repulsion and an intermediate range attraction. These are all generated in the next orders: $\nu = \nu_{min} + 1$ corrections vanish due to parity and time-reversal invariance, but $\nu = \nu_{min} + 2$ corrections are several. First, there are short-range corrections; they come from one-loop pion dressing of the lowest-order contact interactions, and from four-nucleon contact interactions with two derivatives or two powers of the pion mass. It is easy to show that the result of loop diagrams amount to a simple shift of the contact parameters. Second, there are corrections to OPE; these come from vertex dressing and from recoil upon pion emission. Third, there are two-pion exchange (TPE) diagrams built out of lowest-order πNN (and $\pi N\Delta$) interaction. At $\nu = \nu_{min} + 3$ a few more TPE diagrams appear, which involve the $\pi\pi NN$ seagull vertices from the $\Delta = 1$ Lagrangian. To this order there are also small some relativistic corrections. At $\nu = \nu_{min} + 4$ a host of two-loop diagrams and new contact interactions emerge, and so on. Some diagrams are shown in Fig. (14).

A calculation of all contributions to the NN potential up to $\nu = \nu_{min} + 3$ was carried out in Refs. (7, 9) using time-ordered perturbation theory. This EFT potential is energy dependent, but equivalent potentials can be obtained through unitary transformations. An energy-independent potential is more convenient in many situations, and the corresponding version was derived in Ref. (89).

The potential to this order has all the spin-isospin structure of phenomenological models, but its profile is determined by explicit degrees of freedom, symmetries, and power counting. The power counting suggests a hierarchy of short-range effects: S waves should depend strongly on the short-range parameters $C_0^{(S,T)}$; contact interactions affect P -wave phase shifts only in subleading order, so their effect should be smaller and approximately linear; and D and higher waves are directly affected by contact interactions at higher orders, being thus essentially determined by pion exchange. While phenomenological potentials such as that in

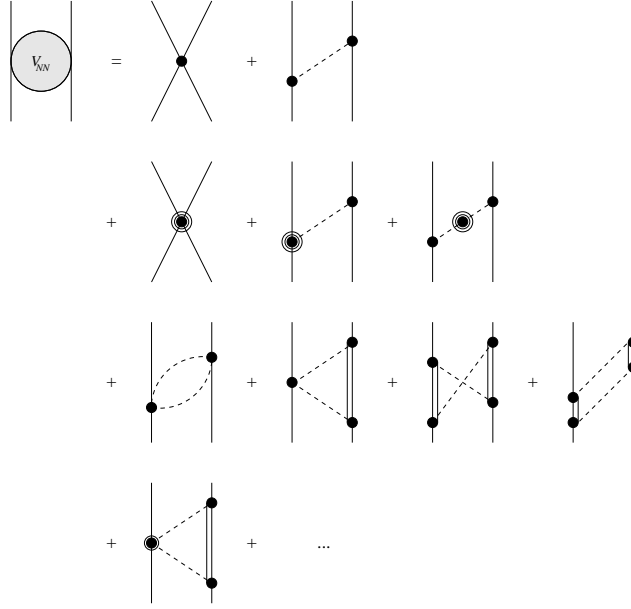


Figure 14: Some time-ordered diagrams contributing to the NN potential in the pionful EFT. (Double) solid lines represent nucleons (and/or deltas), dashed lines pions, a heavy dot an interaction in $\mathcal{L}^{(0)}$, a dot within a circle an interaction in $\mathcal{L}^{(1)}$, and a dot within two circles an interaction in $\mathcal{L}^{(2)}$. The first line corresponds to $\nu = \nu_{min}$, second and third lines to $\nu = \nu_{min} + 2$, fourth line to $\nu = \nu_{min} + 3$, and “...” denote $\nu \geq \nu_{min} + 4$. All orderings with at least one pion (or delta) in intermediate states are included. Not shown are diagrams contributing only to renormalization of parameters.

Ref. (90) have similar short- and long-range structure, it is on TPE that chiral symmetry is particularly influential. TPE here includes a particular form of terms previously considered (91), plus a few new terms. These new terms come from nucleon-structure properties, such as the axial polarizability and the sigma term, and they provide a correlation between the exchanged pions that is important in the isoscalar central force. (Even though graphs where pions interact in flight appear only in next order and should thus be relatively small.) Not surprisingly, in the chiral limit these components of the potential behave at large separations as van der Waals forces. The components of the TPE potential were studied in detail in Ref. (73). In particular, it is shown explicitly that *i*) relativistic corrections are mostly small; *ii*) both isoscalar central and spin-orbit potentials are numerically similar to σ and ω exchange in models; *iii*) the OPE isovector tensor potential is reduced by the TPE contribution. More recently, (the tail of the energy-independent version of) the EFT TPE potential in the limit of a heavy delta was substituted for (the tail of) the one-boson exchange in a Nijmegen phase-shift reanalysis of pp data below 350 MeV (92). A drop in χ^2 was observed. When $\pi\pi NN$ seagull LECs are fitted to the NN data, they come out close to values extracted from πN scattering. This confirms unequivocally the validity of chiral TPE. A new full Nijmegen PSA is in the works, in which chiral TPE is used in the long-range potential (92).

Fits to NN phase shifts were done to this order with (9) and without (78)

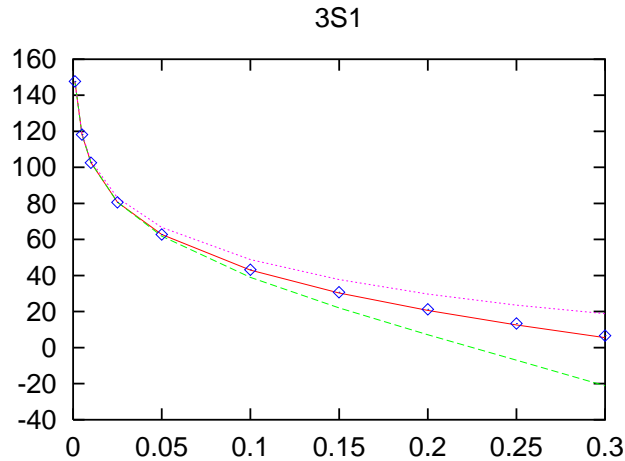


Figure 15: 3S_1 NN phase shift (in degrees) in the EFT with Weinberg counting, as function of the lab energy (in GeV). The (purple) dotted, (green) dashed and (red) solid lines are the results at orders $\nu = \nu_{min}$, $\nu = \nu_{min} + 2$, and $\nu = \nu_{min} + 3$, respectively. The squares are the Nijmegen PSA. From Ref. (78), courtesy of U.-G. Meißner.

explicit delta degrees of freedom. For numerical convenience, smooth cutoffs are used to regulate the loops generated by the Schrödinger equation. For each cutoff value a set of nine independent (bare) parameters stemming from contact interactions were fitted to phase shifts below 100 MeV laboratory energies. However, the fits differed in the details. In Ref. (9), a Gaussian cutoff was used in all loops, and calculations performed with the cutoff parameter Λ taking values 500, 780 and 1000 MeV. In contrast, Ref. (78) used a mixed regularization: while the cutoff parameter in the smooth regulator was varied between 500 and 600 MeV, loops in the potential were treated by a subtraction procedure equivalent to DR. Although OPE and TPE diagrams are completely determined by LECs accessible in πN reactions, most of these LECs were not known at the time of Ref. (9), and were also searched in the fit. In Ref. (78), these parameters were taken from a (DR) fit to πN scattering, which allowed for a simpler, partial-wave-by-partial-wave fit of NN phase shifts. Reasonable agreement with existing PSAs and deuteron properties was found, especially in Ref. (78). As an example, the 3S_1 phase shift at various orders is shown in Fig. (15) and compared to the Nijmegen PSA (26). (Cf. Figs. (2, 10, 13).) The contributions from the short-range parameters in this fit turn out to be comparable to those from heavier resonances in phenomenological models (93).

Although the fits to $\nu = \nu_{min} + 3$ are good, they are inferior to the so-called “realistic” potentials that use 40–50 parameters to fit data up to 300 MeV with a χ^2 near 1. First steps are being made to extend the EFT potential to $\nu = \nu_{min} + 4$. In Ref. (94), contact interactions of this order were added to the complete deltaless $\nu = \nu_{min} + 3$ potential, bringing the number of adjustable parameters to the level of realistic potentials and the Nijmegen PSA. The resulting fit is of quality comparable to realistic potentials. (Indeed, the difference among realistic

potentials arise from high-momentum intermediate states that probe scales which cannot be uniquely fixed by low-energy fits (95).) In order to achieve a complete $\nu = \nu_{min} + 4$ potential, two-loop diagrams and corrections to one-loop diagrams need to be included. Classes of these diagrams that are invariant under pion-field redefinitions have been calculated in Ref. (96). They are compared to peripheral partial waves in Ref. (97), where they are found to be relatively small. We expect to soon witness a complete $\nu = \nu_{min} + 4$ fit of high accuracy.

3.2.4 Isospin violation

The mass difference between u and d quarks breaks isospin symmetry explicitly. Indication from the meson masses is that the ratio $\varepsilon \equiv (m_u - m_d)/(m_u + m_d) \sim 1/3$. Naively, this suggests that isospin might not be a much better symmetry than the rest of the chiral group. On the other hand, a cursory look at hadron masses and a more complete analysis of dynamical amplitudes show that isospin is typically broken only at the few percent level.

Why is isospin such a good symmetry at low energies? The answer can be found in the pattern of chiral-symmetry breaking incorporated in the chiral Lagrangian (11). While explicit chiral-symmetry-breaking effects are present already at index $\Delta = 0$ through the pion mass term, operators generated by the quark mass difference appear only at $\Delta = 1$ through a term that contributes to the nucleon mass splitting and, due to chiral symmetry, to certain pion-nucleon interactions. As a consequence, in most quantities isospin breaking competes with isospin-conserving operators of lower order, and its relative size is not ε but $\varepsilon(Q/M_{QCD})^n$, where n is a positive integer. In other words, isospin is an accidental symmetry (11): a symmetry of the lowest order EFT which is not a symmetry of the underlying theory. The only known exception to this rule is in the isoscalar t channel in πN scattering at threshold. There, there is no contribution from the $\Delta = 0$ Lagrangian, and both the isospin-conserving and -violating amplitudes start at the same order. The isospin-violating piece comes from the pion-nucleon interactions linked to the nucleon mass splitting. Unfortunately, this is hard to see experimentally.

Along these lines, one can study the expected size of isospin breaking in the nuclear potential. We follow the standard nomenclature and refer to an isospin-symmetric potential as “class I”, to a potential that breaks charge dependence but not charge symmetry —defined as a rotation of π around the 2-axis in isospin space— as “class II”, to one that breaks charge symmetry but vanishes in the np system as “class III”, and to one that breaks charge symmetry but causes mixing in the np system as “class IV”.

At $Q \sim M_{NN}$, photon exchanges are perturbative. These standard electromagnetic effects from “soft” photons can be obtained straightforwardly from gauge-invariant operators involving the photon field. In addition, isospin violation arises from the quark masses, from indirect electromagnetic effects, and from simultaneous pion-photon exchange. In order to compare the various sources of isospin breaking, we note that the size of electromagnetic effects in loops is typically $\sim \alpha/\pi$ which, numerically, is $\sim \varepsilon(Q/M_{QCD})^3$.

The leading isospin-breaking interactions in Weinberg’s power counting have been derived in Ref. (11). (The necessary modification of Weinberg’s counting discussed in Sect. 3.2.2 shows that chiral-symmetry-breaking terms are even more suppressed *vis-a-vis* chiral-symmetric ones, and is not expected to affect the

relative sizes among isospin-breaking interactions.) No isospin-violating effects appear at leading order, $\nu = \nu_{min}$, so the leading potential is class I. The first isospin-breaking effect (in addition to Coulomb exchange) appears at $\nu = \nu_{min} + 1$ in the form of a class II isospin violation from the pion mass splitting ($\Delta m_\pi^2 = \mathcal{O}(\alpha M_{QCD}^2/\pi)$) in OPE. One order down, $\nu = \nu_{min} + 2$, a class III force appears mainly from the quark mass difference through breaking in the πNN coupling ($\beta_1 = \mathcal{O}(\varepsilon m_\pi^2/M_{QCD}^2)$) in OPE, from contact terms ($\gamma_{s,\sigma} = \mathcal{O}(\varepsilon m_\pi^2/M_{QCD}^4)$), and from the nucleon mass difference ($\Delta m_N = \mathcal{O}(\varepsilon m_\pi^2/M_{QCD})$). To this order the isospin-violating nuclear potential is a two-nucleon potential of the form

$$V_{ib} = V_{II} [(t_1)_3(t_2)_3 - \mathbf{t}_1 \cdot \mathbf{t}_2] + V_{III} [(t_1)_3 + (t_2)_3], \quad (54)$$

where

$$V_{II} = - \left(\frac{g_A}{f_\pi} \right)^2 \frac{\vec{q} \cdot \vec{\sigma}_1 \vec{q} \cdot \vec{\sigma}_2}{(\vec{q}^2 + m_{\pi^0}^2)(\vec{q}^2 + m_{\pi^\pm}^2)} (\Delta m_\pi^2 + \Delta m_N^2), \quad (55)$$

$$V_{III} = \frac{g_A \beta_1}{2f_\pi^2} \frac{\vec{q} \cdot \vec{\sigma}_1 \vec{q} \cdot \vec{\sigma}_2}{\vec{q}^2 + m_\pi^2} - (\gamma_s + \gamma_\sigma \vec{\sigma}_1 \cdot \vec{\sigma}_2). \quad (56)$$

Finally, class IV forces appear only at order $\nu = \nu_{min} + 3$.

We conclude that the pattern of symmetry breaking in QCD naturally suggests a hierarchy of classes in the nuclear potential (11):

$$\frac{\langle V_{M+1} \rangle}{\langle V_M \rangle} \sim \mathcal{O} \left(\frac{Q}{M_{QCD}} \right), \quad (57)$$

where $\langle V_M \rangle$ denotes the average contribution of the leading class M potential. This qualitatively explains not only why isospin is a good approximate symmetry at low energies, but also why charge symmetry is an even better symmetry. It gives, for example, the observed isospin structure of the Coulomb-corrected scattering lengths (98), $a_{np} \simeq 4 \times ((a_{nn} + a_{pp})/2 - a_{np}) \simeq 4^2 \times (a_{pp} - a_{nn})$.

One can use the above formalism to do consistent and systematic calculations of isospin violation. For example, the isospin-violating potential of ranges $\sim 1/m_\pi$ and $\sim 1/2m_\pi$ up to $\nu = \nu_{min} + 3$ were computed in Refs. (99, 100, 101). In contrast to previous attempts lacking an EFT framework, the EFT results are invariant under both gauge transformation and pion-field redefinition and have simple forms. The component of range $\sim 1/m_\pi$ comes from diagrams with all possible one-photon dressings of OPE, plus the relevant counterterms (99). Its isospin structure allows only charged-pion exchange and therefore is class II. This $\pi\gamma$ potential has been incorporated in a Nijmegen phase shift reanalysis of np data below 350 MeV (99). We can use the values for the πNN coupling constants determined by the analysis to find that their isospin breaking (β_1) is consistent with zero, with an uncertainty comparable to our expectation from dimensional analysis and from $\pi - \eta - \eta'$ mixing (102). Similarly, the two contact interactions ($\gamma_{s,t}$) might be viewed as originating in $\rho - \omega$ mixing and pseudovector-meson exchange (in particular close-lying doublets such as $a_1 - f_1$) (102, 103). The components of range $\sim 1/2m_\pi$ come from two sources. One is the pion mass difference (Δm_π^2) in TPE that generates a class II potential (100); the other is a $\pi\pi NN$ seagull that arises as a chiral partner of the nucleon mass difference (Δm_N), and produces a class III TPE potential (101). All these effects are relatively small, with estimated contributions to the scattering lengths of $\sim \pm 0.5$

fm. These long-range components could be included in the new Nijmegen PSA (92).

A fit to NN phase shifts including various isospin-breaking interactions was carried out in Ref. (104), improving on an earlier analysis with perturbative pions (105). A slightly different counting is used that enhances by one order the electromagnetic effects, electromagnetic corrections being counted as $\alpha \sim (Q/M_{QCD})^2$. The EFT potential to order $\nu = \nu_{min} + 2$ (including Coulomb) is then fitted to low-energy S and P , np and pp phase shifts, using cutoffs in the range 300 – 500 MeV. With modest cutoff dependence, isospin breaking in the scattering lengths can be accommodated, and higher energies and partial waves predicted. A next-order calculation should achieve the level of precision of modern phenomenological potentials.

3.3 Three- and four-nucleon systems

When few-body systems are considered, one needs to address the issue of few-body forces, which, being in general not forbidden by symmetries, will at some level contribute to observables. One of the advantages of a field-theoretical framework is the possibility of the derivation of consistent few-body forces, free of off-shell ambiguities. In the standard nuclear-physics approach, few-nucleon forces are either inspired by arguments that are independent of the assumptions invoked in the NN potential, or simply guessed on phenomenological terms.

The pionful EFT offers some insight into few-nucleon forces. In addition to contact interactions as in the pionless theory, one has further pion-exchange components. The potential, being defined as a sub-amplitude, includes (for $A > 2$) diagrams that have $C \geq 1$ separately connected pieces. An n -nucleon force is a contribution to the *potential* that connects n nucleons.

Weinberg's power counting embodied in Eq. (43) suggests a hierarchy of few-nucleon forces. As in the two-nucleon case, this power counting relies on an implicit assumption about the scale appearing in contact interactions. We have seen in Sect. 2.2.2 that in the pionless EFT the running of the renormalization group toward low energies enhances the size of three-body forces. The latter get contaminated by the fine-tuning present in the two-body sector. Whether the same happens at the higher energies relevant to the pionful theory is not clear. Part of the $3N$ forces in the pionless theory match onto diagrams of the pionful theory which are the iteration of the NN potential (through NN intermediate states where at least one nucleon has momentum $\mathcal{O}(m_\pi)$). It is conceivable that the enhancement is removed from contact interactions once the pion is introduced explicitly in the EFT.

The new forces that appear in systems with more than two nucleons have been derived in Refs. (7,8,10). The dominant potential, at $\nu = 6 - 3A = \nu_{min}$, is simply the NN potential of lowest order that we have already encountered in Sect. 3.2.3. We can easily verify that, if the delta is kept as an explicit degree of freedom, a $3N$ potential will arise at $\nu = \nu_{min} + 2$, a $4N$ potential at $\nu = \nu_{min} + 4$, and so on. It is (approximate) chiral symmetry therefore that implies that n -nucleon forces V_{nN} obey a hierarchy of the type

$$\frac{\langle V_{(n+1)N} \rangle}{\langle V_{nN} \rangle} \sim \mathcal{O} \left(\frac{Q}{M_{QCD}} \right)^2, \quad (58)$$

with $\langle V_{nN} \rangle$ denoting the contribution per n -plet. (This hierarchy is a non-trivial

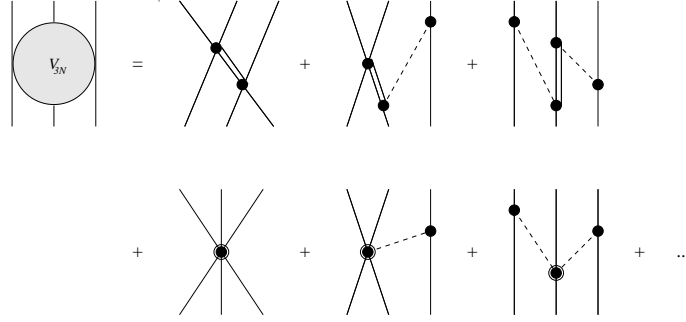


Figure 16: Some time-ordered diagrams contributing to the $3N$ potential in the pionful EFT. (Double) solid lines represent nucleons (and/or deltas), dashed lines pions, a heavy dot an interaction in $\mathcal{L}^{(0)}$, and a dot within a circle an interaction in $\mathcal{L}^{(1)}$. First line corresponds to $\nu = \nu_{min} + 2$, second line to $\nu = \nu_{min} + 3$, and “...” denote $\nu \geq \nu_{min} + 4$. All nucleon permutations and orderings with at least one pion or delta in intermediate states are included.

The leading $3N$ potential (10) has components with three different ranges: TPE; OPE/short-range; and purely short ranged. (Relativistic corrections neglected below are discussed in Ref. (74).) The TPE part of the potential is determined in terms of πN scattering observables (10). It is similar to the Tucson-Melbourne (TM) and Brazil potentials (109), but it corrects a deficiency of the TM potential in regard to chiral symmetry. The TM potential was built from a πN scattering amplitude that corresponds to a particular choice of pion fields for which chiral symmetry is not respected term by term (110). Although the on-shell TM πN amplitude agrees with that obtained in EFT to sub-leading order, they differ off shell. Of course, in a field theory the corresponding $3N$ potentials involve other interactions that enforce chiral symmetry and invariance under pion-field redefinitions. Unfortunately the original TM potential was not derived within field theory, and the required extra terms were not included. After this is done, the EFT result is obtained (110). The resulting TM’ potential is similar to the Brazil potential, and has been studied in detail in Refs. (112,111). In Ref. (112) it was shown that one of the components of the force is dominant in $3N$ elastic scattering observables. This explains why all existing TPE $3N$ forces give essentially the same results for the $3N$ continuum after being fitted to the triton energy. This type of $3N$ force does not improve agreement for A_y much (112).

The novel OPE/short-range components of the potential involve two $\pi(\bar{N}N)^2$ interactions of strengths not determined by chiral symmetry alone (10). These parameters can be thought of as representing short-range effects such as σ and ω exchanges with an intermediate $N(1440)$ resonance, and ρ exchange from a $\pi\rho$ Kroll-Ruderman term (113). It can be shown that due to the antisymmetry of the wave-function only one combination of parameters contributes (114). This combination can be determined from reactions involving only two nucleons, as discussed in Sect. 3.4 below. In Ref. (112) the effect of these novel terms was estimated assuming that their LECs have natural size. In conjunction with TM’, this force can bridge a significant part of the discrepancy between “realistic” NN potentials and A_y data. Although not a consistent EFT calculation, this

estimate serves to assess the size of $3N$ forces in the EFT. Clearly, agreement with A_y data at $\nu = \nu_{min} + 2$ in the deltaless EFT is purely accidental. Conversely, a full $\nu = \nu_{min} + 3$ calculation might resolve the A_y puzzle.

The purely short-range components of the potential can only be determined from few-nucleon systems (10). As we have seen in Sect. 2.2, the Pauli principle leads to a single LEC. Once this LEC is determined from one $3N$ input (such as the triton binding energy), all other observables (such as A_y) can be predicted (once the OPE/short-range component has been fixed by data involving just two nucleons).

It is apparent that the pionful EFT brings new forces into play, and that these new elements might resolve remaining issues in the description of data. This prospect calls for a fully consistent $\nu_{min} + 3$ calculation with maximal NN input.

3.4 Processes with external probes

The power counting arguments of Sect. 3.2.2 can be easily generalized to the case where external probes with momenta $Q \sim M_{NN}$ interact with few-nucleon systems. The probes deposit an energy $\sim M_{NN}$ onto the nuclear system, so that, if we define the kernel K as the sum of irreducible diagrams to which the probes are attached, the power counting Eq. (43) applies equally well to K . Interactions among nucleons occurring before or after scattering can be treated as before: iteration of the potential gives rise to the wave-function $|\psi\rangle$ ($|\psi'\rangle$) of the initial (final) nuclear state. The full scattering amplitude is then

$$T = \langle \psi' | K | \psi \rangle. \quad (59)$$

The pionful EFT can also handle scattering at smaller Q , of course, but then Eqs. (43, 59) have to be modified. When the deposited energy is $\sim M_{NN}^2/m_N$ —for example, when the incoming probes are photons of momenta $Q \sim M_{NN}^2/m_N$ —there can be intermediate few-nucleon states that are reducible, and the breakdown of T into kernel and wave-functions is more complicated (115). In this situation a perturbative treatment of pions, or even better, the pionless EFT, should suffice.

In practice, it is frequently desirable to minimize nuclear wave-function errors by using a high-precision phenomenological potential. That this is a good approximation is suggested by a comparison (76) between a simplified version of the EFT potential of Ref. (9) and the Argonne V18 potential (90), which show agreement in most aspects of the wave-function. The cost of this “hybrid approach” (8) is the introduction of an uncontrolled error due to a possible mismatch between the off-shell extensions of the kernel and the potential. This error can, on the other hand, be estimated by the use of several different phenomenological potentials of similar quality.

As with few-nucleon forces, the factor $-2C$ in Eq. (43) implies that external probes tend to interact predominantly with a single nucleon, simultaneous interactions with more than one nucleon being suppressed by powers of $(Q/M_{QCD})^2$. Again, this generic dominance of the impulse approximation is a well-known result that arises naturally here. This is of course what allows extraction, to a certain accuracy, of one-nucleon parameters from nuclear experiments. A valuable by-product of the EFT is to provide a consistent framework for one- and few-nucleon dynamics, whereby few-nucleon processes can be used to infer one-nucleon properties. More interesting from the purely nuclear-dynamics perspective are, how-

ever, those processes where the leading single-nucleon contribution vanishes by a particular choice of experimental conditions, for example the threshold region. In this case, certain two-nucleon contributions, especially in the relatively large deuteron, can become important. Further examination of the structure of the chiral Lagrangian reveals that two-nucleon contributions tend to be dominated by pion exchange. Indeed, photons and pions couple to four-nucleon operators only at $\mathcal{O}(Q/M_{QCD})$ relative to pion-exchange diagrams constructed out of the leading-order Lagrangian. Thus power counting justifies the ‘‘chiral filter hypothesis’’ that was put forward to summarize some empirical results on electroweak form factors (116). This ‘‘pion dominance’’ ensures that two-nucleon contributions from the EFT in lowest orders tend to be similar to those in phenomenological models that include pion-exchange currents.

Many processes have been analysed in the pionful EFT. Some of those processes are extensions to higher energies of the same electroweak processes described in Sect. 2.1. For example,

- $ed \rightarrow ed$ and deuteron form factors (117)
- $\vec{e}d \rightarrow eNN$ and parity violation (118)
- $np \rightarrow d\gamma$ and meson-exchange currents (119)
- $\vec{n}p \rightarrow d\gamma$ and parity violation (120)
- $pp \rightarrow de^+\nu_e$ and axial currents (121)
- $p\ ^3\text{He} \rightarrow\ ^4\text{He}\ e^+\nu_e$ and solar neutrino production (122)
- $\nu d \rightarrow lNN$ and solar neutrino detection (123)
- $\mu d \rightarrow \nu_\mu nn$ and its measured rate (124)
- $\gamma d \rightarrow \gamma d$ and nucleon polarizabilities (125, 115)

For details, we refer the reader to more extensive reviews (18) and the original papers. Here we briefly discuss those processes more germane to the pionful theory, involving pions in initial and/or final states.

3.4.1 $\pi d \rightarrow \pi d$

This is perhaps the most direct way to check the consistency of EFT in one- and few-nucleon systems. For simplicity, consider the region near threshold with the delta integrated out. There the lowest-order, $\nu = \nu_{min} = -2$ contributions to the kernel vanish because the pion is in an s wave and the target is isoscalar. The $\nu = \nu_{min} + 1$ term comes from the (small) isoscalar pion-nucleon seagull, related in lowest-order to the pion-nucleon isoscalar amplitude $b^{(0)}$. $\nu = \nu_{min} + 2$ contributions come from corrections to πN scattering and two-nucleon diagrams, which involve besides $b^{(0)}$ also the much larger isovector amplitude $b^{(1)}$. These various contributions to the πd scattering length have been estimated (8, 126). They were found in agreement with previous, more phenomenological calculations, which have been used to extract $b^{(0)}$. Partial sets of higher-order corrections have been evaluated in Ref. (127) (and in Ref. (128) for the related, double-charge-exchange process). A consistent $\nu = \nu_{min} + 3$ calculation of πd elastic scattering is in progress (129). Eventually, a $\nu = \nu_{min} + 4$ calculation might be required in order to determine the chiral-symmetry breaking LEC $C_2^{(qm)}$ discussed further below in connection with lattice QCD. Charge-symmetry-breaking effects were considered in Ref. (130). Note that an alternative approach with perturbative pions (131) also seems to accommodate the available experimental data.

3.4.2 $\gamma^{(*)}d \rightarrow \pi^0 d$

This reaction offers the possibility to test a prediction arising from a combination of two-nucleon contributions and the single-neutron amplitude. The differential cross section for a photon of momentum k and longitudinal polarization ϵ_L to produce a pion of momentum q is, at threshold,

$$\left[\left(\frac{3k}{8q} \right) \left(\frac{d\sigma}{d\Omega} \right) \right]_{q=0} = |E_d|^2 + \epsilon_L |L_d|^2, \quad (60)$$

where the electric dipole amplitude $E_d(k^2)$ characterizes the transverse response and $L_d(k^2)$ the longitudinal response.

$E_d(0)$ was studied up to $\nu = \nu_{min} + 3$ with the delta integrated out in Ref. (132). There are two classes of contributions, according to whether the external light particles interact with one or with both nucleons. The one-nucleon part of the kernel is given by standard $A = 1$ ChPT, with due account of P waves and Fermi motion inside the deuteron. The neutrality of the outgoing s -wave pion ensures that the leading $\nu = -2 = \nu_{min}$ terms vanish. The first two-nucleon part of the kernel appears at $\nu = \nu_{min} + 2$; it comes from a virtual charged pion photoproduced on one nucleon which rescatters on the other nucleon with charge exchange. These contributions are actually numerically larger than indicated by power counting due to the relatively large deuteron size. Smaller two-nucleon terms appear at $\nu = \nu_{min} + 3$ from corrections in either nucleon. Results for $E_d(0)$ up to $\nu = \nu_{min} + 3$ (132) are shown in Table 2. They correspond to the Argonne V18 potential (90) and a cutoff $\Lambda = 1000$ MeV. Other realistic potentials and cutoffs from 650 to 1500 MeV give the same result within 5%. The chiral potentials of Sect. 3.2.3 are more cumbersome to use, but it has been verified that they give results that are similar to other potentials. Two-nucleon contributions seem to be converging, although more convincing evidence would come from next order, where loops appear. A model-dependent estimate (133) of some $\nu = \nu_{min} + 4$ terms suggests a 10% or larger error from neglected higher orders in the kernel itself. The single-scattering contribution depends on the amplitude for $\gamma n \rightarrow \pi^0 n$, $E_{0+}^{(\pi^0 n)}$, in such a way that $E_d(0) \sim -1.79 - 0.38(2.13 - E_{0+}^{(\pi^0 n)})$ in units of $10^{-3}/m_{\pi^+}$. Thus, sensitivity to $E_{0+}^{(\pi^0 n)}$ survives the large two-nucleon contribution at $\nu = \nu_{min} + 2$.

We see that working within the EFT yields a testable prediction, $E_d(0) = -(1.8 \pm 0.2) \cdot 10^{-3}/m_{\pi^+}$ (132). It is remarkable that for this process EFT gives results that are significantly different from tree-level models of the type traditionally used in nuclear physics. For example, the models in Ref. (134) predict the threshold cross section about twice as large as the EFT. Most of the dif-

Table 2: Values for $E_d(0)$ in units of $10^{-3}/m_{\pi^+}$ from one-nucleon contributions (1N) up to $\nu = \nu_{min} + 3$, two-nucleon kernel (2N) at $\nu = \nu_{min} + 2$ and at $\nu = \nu_{min} + 3$, and their sum (1N + 2N).

1N	2N		1N + 2N
$\nu \leq \nu_{min} + 3$	$\nu = \nu_{min} + 2$	$\nu = \nu_{min} + 3$	$\nu \leq \nu_{min} + 3$
0.36	-1.90	-0.25	-1.79

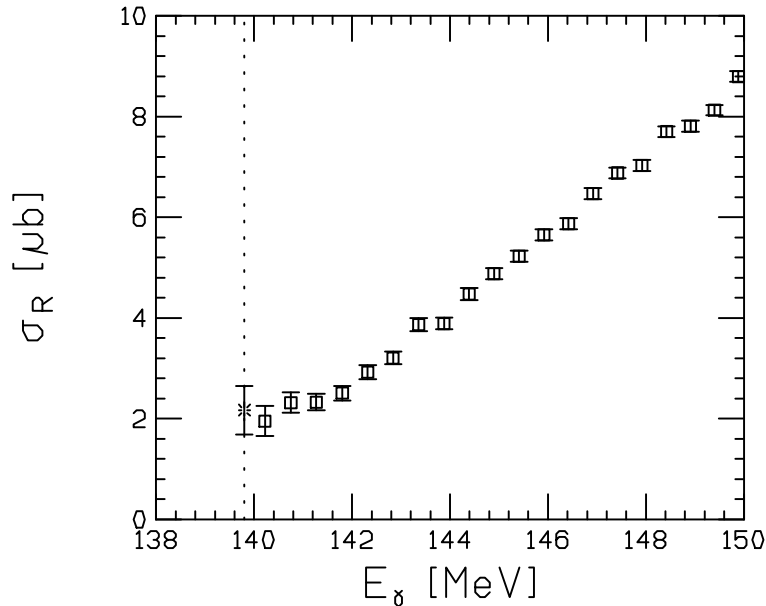


Figure 17: Reduced cross section $\sigma_R = (k/q)\sigma$ for neutral-pion photoproduction as function of the photon energy. Threshold is marked by a dotted line. The star at threshold is the EFT prediction (132), and squares are data points (135). Figure courtesy of U.-G. Meißner.

ference comes from one-nucleon loop diagrams: tree-level models tend to differ from ChPT mostly by having a smaller $E_{0+}^{(\pi^0 n)}$, which increases $|E_d|$. A test of this prediction is thus an important check of our understanding of the role of QCD at low energies. Such a test was carried out at Saskatoon (135). The experimental results for the pion photoproduction cross section near threshold are shown in Fig. (17), together with the EFT prediction at threshold (132). Inelastic contributions have been estimated in Refs. (135,136) and are smaller than 10% throughout the range of energies shown. At threshold, Ref. (135) finds $E_d(0) = -(1.45 \pm 0.09) \cdot 10^{-3}/m_{\pi^+}$. While agreement with the EFT to order $\nu = \nu_{min} + 3$ is not better than a reasonable estimate of higher-order terms, it is clearly superior to tree-level models. This is compelling evidence of chiral loops.

A further test of the EFT comes from the coherent neutral-pion electroproduction on the deuteron. $E_d(k^2)$ and $L_d(k^2)$ were predicted to $\nu = \nu_{min} + 2$ (with no new free parameters) in Ref. (137), for transferred momenta in the range $0 - 0.1 \text{ GeV}^2$. Because $E_{0+}^{(\pi^0 p)}$ is not well reproduced at this order, only the k^2 dependence can be tested. This reaction was measured at $k^2 = -0.1 \text{ GeV}^2$ in Mainz (138), and values for $|E_d(-0.1)|$ and $|L_d(-0.1)|$ were extracted. If they are compared with the results from Ref. (137) simply shifted by a k^2 -independent amount in order to reproduce the $E_d(0)$ of the $\nu = \nu_{min} + 3$ calculation, then there is good agreement for $|E_d(-0.1)|$ but $|L_d(-0.1)|$ fails by a factor 2 (138). Because the calculated $L_d(k^2)$ is not dominated by a single mechanism to the extent $E_d(k^2)$ is, it is possible that it suffers from stronger corrections in next order. An extension of these calculations to higher order and beyond threshold is also highly desirable.

3.4.3 $NN \rightarrow NN\pi$

This reaction has attracted a lot of interest because of the failure of standard phenomenological mechanisms in reproducing the small cross section observed near threshold. It involves larger momenta of $\mathcal{O}(\sqrt{m_\pi m_N})$, so the relevant expansion parameter here is not so small, $(m_\pi/m_N)^{\frac{1}{2}}$. This process is therefore not a good testing ground for the above ideas. But $(m_\pi/m_N)^{\frac{1}{2}}$ is still < 1 , so at least in some formal sense we can perform a low-energy expansion. In Refs. (139, 140) the chiral expansion was adapted to this reaction and the first few contributions estimated. (Note that —contrary to what is stated in Ref. (141)— momenta $\sim \sqrt{m_\pi m_N}$ do not necessarily imply a breakdown of the non-relativistic expansion, as $p^4/m_N^3 \sim (m_\pi/m_N)(p^2/m_N)$ is still small.)

Initial attention concentrated on $pp \rightarrow pp\pi^0$ at threshold. The lowest-order terms all vanish, and the formally-leading non-vanishing terms—an impulse term and a similar diagram from the delta isobar—are anomalously small and partly cancel. The bulk of the cross section must then arise from contributions that are relatively unimportant in other processes: isoscalar pion rescattering, TPE, and high-order short-range $\pi(\bar{N}N)^2$ terms. While the first two contributions are calculable, the third involves LECs that can only be fitted or modeled. These LECs can be thought of as originating from heavier-meson exchange: pair diagrams with σ and ω exchange, and a $\pi\rho\omega$ coupling, among other, smaller terms (142). In Ref. (142) it was shown that a large uncertainty comes from the short-range features of the wave-function, so a more systematic study has to await the development of chiral potentials that are accurate at the relevant energies. Other EFT studies of this channel, including attempts to compute TPE, can be found in Ref. (143). More problematic is the situation with the threshold cross section of other, not so suppressed channels $NN \rightarrow d\pi, \rightarrow pn\pi$. In those channels the Weinberg-Tomozawa $\pi\pi NN$ term, fixed by chiral symmetry, dominates. Wave-function dependence is much smaller, yet a calculation including leading and some sub-leading contributions underpredicts the data by a factor of ~ 2 (144). A calculation including TPE is badly needed.

Despite these problems, much can be learned from this reaction in the threshold region. One example is charge-symmetry breaking. The nucleon mass splitting comes from both the quark mass difference and from electromagnetic effects, $\Delta m_N = \delta m_N + \bar{\delta} m_N$, with $\delta m_N = \mathcal{O}(\varepsilon m_\pi^2/M_{QCD})$ and $\bar{\delta} m_N = \mathcal{O}(\alpha M_{QCD}/\pi)$. Determining the two LECs δm_N and $\bar{\delta} m_N$ separately is interesting for several reasons: coupled to a lattice evaluation of δm_N , it can be used to extract quark masses; it can test quark models that evaluate $\bar{\delta} m_N$; and it can constrain a possible time variation of α because ${}^4\text{He}$ nucleosynthesis is sensitive to Δm_N . These LECs contribute in combinations other than Δm_N to processes involving pions, because the two operators that generate the nucleon mass difference have different chiral partners, which involve an even number of pions. Unfortunately, these LECs are hard to measure directly in πN scattering. The forward-backward asymmetry in $np \rightarrow d\pi^0$, on the other hand, is sensitive to the charge-symmetry breaking from these operators, and it has been calculated (145). Since the asymmetry is related to a ratio of amplitudes, some of the uncertainties in the strong-interaction physics are reduced. The asymmetry is being measured at TRIUMF (146), at a level that could allow for an observation of the quark-mass-difference effect. A related experiment, $dd \rightarrow \alpha\pi^0$, which can address the same issues but with different theoretical uncertainties, has been proposed at IUCF (147).

It is possible that some of the problems encountered at threshold stem from the smallness of pion s waves, which show poor convergence also in $A = 1$ ChPT—for example, in neutral pion photoproduction on the proton. Indeed, p -wave pion production seems better behaved. Ref. (140) calculates the first two orders of the cross section for the $pp \rightarrow pp\pi^0$ reaction with initial nucleons in the spin $S = 1$ state in the direction of the incoming center-of-mass momentum, as function of the outgoing pion momentum in the range $0.5 - 1 m_\pi$. With no free parameters, good convergence and reasonable agreement with data are found. It was also pointed out that other observables would, at that order, be sensitive to a combination of $\pi(\bar{N}N)^2$ LECs that affects the leading $3N$ force, discussed in Sect. 3.3. In particular, the amplitude for the ${}^1S_0 \rightarrow ({}^3S_1 - {}^3D_1)p$ transition, which vanishes in leading order, is very sensitive to this LEC. This amplitude, extracted from the $pp \rightarrow pn\pi^+$ data for pion momenta in the range $0.2 - 0.5 m_\pi$, can be fitted quite well with a natural-sized LEC (140). This value for the LEC can be used in the $3N$ potential to improve the predictive power of the chiral potential.

All calculations of pion-production observables have involved approximations necessary to match the kernel and wave-functions. A critical discussions of these approximations can be found in Ref. (148). Issues such as the size of the contribution of the πNN cut, not well accounted for in the common approximations, need to be better understood. Pion production is clearly wide open for further development.

3.5 Connection with lattice QCD

The holy grail of nuclear physics has for some time been its derivation from QCD. As we have seen, light nuclei are large objects of size $\sim 1/M_{NN} \gg 1/M_{QCD}$, or larger. Dynamics at this scale can be understood within the EFT, and all nuclear information is encoded in the parameters of the EFT Lagrangian. These parameters, in turn, are fixed by the physics of smaller distances. If the EFT can somehow be matched onto QCD at some scale not far below M_{QCD} , the EFT can be used to predict all of traditional nuclear physics. The EFT allows to split the quest for the holy grail in two stages, according to the two energy scales.

At present, the best hope for a solution of QCD in the regime of large coupling constant relevant for nuclear physics is by explicit numerical solution on the lattice. However, the large size of nuclei make their direct simulation practically and intellectually unsound. A more reasonable goal for is to match with the EFT, which requires lattices of size not much larger than $1/M_{QCD}$. We are still far from this goal, but a few steps have already been taken.

One obstacle arises from the difficulty in simulating small pion masses. For example, Ref. (149) computes the 1S_0 and 3S_1 scattering lengths in quenched QCD with $m_\pi \gtrsim 500$ MeV.

The m_π dependence of nuclear forces comes in explicitly from pion propagators in pion exchange, and implicitly from short-range interactions. For illustration, in Fig. (18) we exhibit the deuteron binding energy and the 3S_1 scattering length stemming from the leading *explicit* m_π dependence in the expansion around the chiral limit (83). A higher-order two-derivative contact interaction was also included and fitted to the triplet effective range. For the physical value of the pion mass, one gets the deuteron binding energy to reasonable accuracy, $B_d = 2.211$ MeV (essentially independent of the cutoff R). In the chiral limit

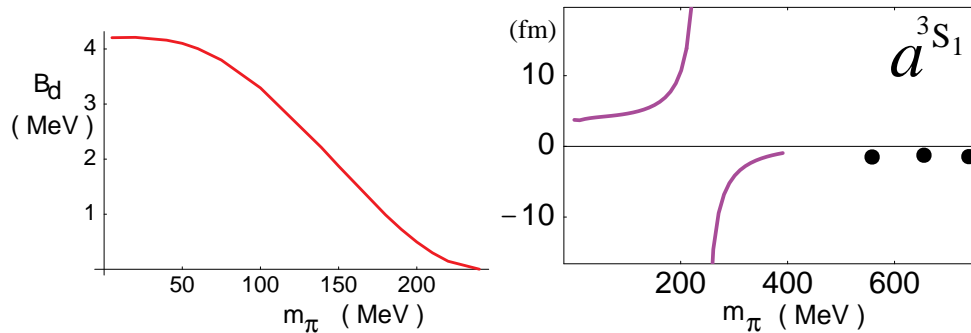


Figure 18: The deuteron binding energy (left panel) and the 3S_1 scattering length (right panel) as functions of the pion mass that explicitly appears in the OPE potential. Implicit pion-mass dependence was not calculated, as other parameters were set to their physical values for all m_π . The dots are quenched lattice QCD data. From Ref. (83).

the deuteron is bound by $B_d^0 \simeq 4.2$ MeV. This value is still somewhat small compared to $f_\pi^2/2m_N \sim 10$ MeV, which one might expect to arise in QCD, and therefore one would conclude that the deuteron is still weakly bound in the chiral limit! This calculation of the explicit m_π dependence agrees with that obtained with the AV18 potential (150) with $m_\pi = 0$, of $B_d^{0(AV18)} \simeq 4.1$ MeV. The lattice data for the triplet scattering length from Ref. (149) are also shown.

While phenomenological models typically can only vary m_π in OPE, all aspects of m_π dependence can in principle be determined in the pionful EFT. Since the pion mass can be varied up to M_{QCD} , the EFT can be used to extrapolate lattice results to realistic values of m_π . It was pointed out in Ref. (83) that the leading (explicit *and implicit*) m_π dependence of nuclear forces can be calculated once the chiral-symmetry-breaking LEC $C_2^{(qm)}$ is known. That is because the leading m_π dependence in f_π , g_A and m_N is known from ChPT. Unfortunately, determination of $C_2^{(qm)}$ requires calculation of processes involving external pions —e.g. πd scattering, see Sect. 3.4.1— at high orders and, consequently, precise low-energy data. Alternatively, one can imagine fitting $C_2^{(qm)}$ to the lattice data themselves.

Note that in Fig. (18) we illegally compared the EFT with quenched QCD. Most simulations cannot yet be done in QCD itself, but only in quenched or, more generally, partially-quenched QCD (PQQCD), where different masses are assigned to valence and sea quarks. PQQCD has a different symmetry pattern than QCD, a different low-energy dynamics, and thus a different dependence on the pion mass. A proper extrapolation of PQQCD data to smaller pion masses requires a partially-quenched EFT. Implications of PQEFT to the NN interaction are discussed in Ref. (151).

4 OUTLOOK

4.1 More-nucleon systems

We have seen that the EFT paradigm has been extensively applied to systems with $A = 2 - 4$, for momenta below and above the pion mass. Work remains to be done even for those systems, of course. For example, the chiral expansion of the pionful EFT still needs to be better understood for $A = 2, 3$; and $A = 4$ has to be studied in the pionless EFT in order to uncover the role of a $4N$ force that could appear in LO.

As these issues get settled, a natural next step for the EFT program is to increase A . There have, in fact, been attempts to extend the paradigm to heavier nuclei.

For example, EFT methods are being used to perfect the nuclear shell model (152). The goal here is to take some modern potential model and simplify the bound-state problem for large nuclei in such a way as to make a numerical solution of the Schrödinger equation feasible. This simplification comes about by reducing the dimensionality of the original Hilbert space of the shell model, the effect of the highly excited states being included into local operators acting on a reduced Hilbert space. The reduced problem obtained by “integrating out” the high-energy modes can then be solved by standard numerical methods.

Another approach is to develop an EFT to handle other nuclei that are, like the deuteron, particularly shallow (153). Examples are halo nuclei, where the separation energy of one or more nucleons is much smaller than the energies associated with a core of the remaining nucleons.

There have also been many EFT-inspired studies of nuclear matter ($A \rightarrow \infty$, $\alpha = 0$) and very heavy nuclei. They have all aimed at identifying the relevant degrees of freedom and an expansion parameter that can describe physics for densities around the saturation density. See, for example, Ref. (154).

Whether these approaches prove to be *bona fide* EFTs (in the sense used in this review) or not, the problem remains of deriving the saturation of nuclear matter from an EFT adjusted to describe few-nucleon physics. This is a formidable problem: the complexity of the necessary resummations of LO operators increases rapidly with A , becoming high already at $A = 5$. Lacking the identification of a further expansion parameter, we might, as in QCD itself, have to resort to lattice simulations. A step in this direction was taken in Ref. (155), where a toy model with no- and two-derivative contact two-body interactions was solved (at zero and at finite temperature) on a spatial lattice using Monte Carlo techniques, and the interaction parameters were fitted to saturation properties. The next step involves using EFT interactions determined from few-nucleon systems.

These attempts, interesting as they are, fall outside the scope of this review, and we refer the reader to the original literature.

4.2 Conclusion

For the last couple of years, the pionless EFT has been developed and applied to two- and three-nucleon systems. Although for the NN system in isolation it amounts to nothing more than ERT, the full power of the field-theory arsenal comes to fruition when more nucleons and/or external probes are considered. We have seen that the extension to the $3N$ system is full of surprises, such as the appearance of limit-cycle behavior and of a relevant three-body force. These surprises have been turned into successes, and relatively simple calculations yield

results of quality not inferior to polished potentials models. Although limited in energy, this EFT can achieve high precision for reactions of interest to astrophysics, such as $np \rightarrow d\gamma$.

The older pionful EFT is less well understood. There are hints that the expansion has finally been identified as an expansion around the chiral limit, but higher orders in the expansion must be studied. Among the higher-order terms is a LEC, $C_2^{(qm)}$, that is the main uncertainty in the extrapolation to the chiral and heavy-pion limits. External probes might be able to determine this LEC. Anyhow, considerable progress has been achieved in the development of the EFT NN potential. Isospin-violating effects are a unique virtue of the pionful EFT because they are so tightly linked to the pattern of QCD symmetries. There remain issues regarding the size of short-range $3N$ forces, but novel longer-range $3N$ forces naturally appear and can play an important role in nuclear dynamics. An assessment of this progress from the perspective of the historical development of nuclear potentials can be found in Ref. (156).

Yet, most nuclei still await us.

Acknowledgments

We would like to thank our collaborators for teaching us most of what we know about effective theories and nuclear physics. UvK is grateful to the Nuclear Theory Groups at the U of Washington, U of South Carolina, Ohio U and Ohio State U, and to the INT for hospitality during stages of the writing of this paper. Thanks to RIKEN, Brookhaven National Laboratory and to the U.S. Department of Energy [DE-AC02-98CH10886] for providing the facilities essential for the completion of this work. This work was supported by the Director, Office of Energy Research, Office of High Energy and Nuclear Physics, and by the Office of Basic Energy Sciences, Division of Nuclear Sciences, of the U.S. Department of Energy under Contract No. DE-AC03-76SF00098 (PFB), and by a DOE Outstanding Junior Investigator Award (UvK).

Literature Cited

1. Manohar AV. hep-ph/9606222; Kaplan DB. nucl-th/9506035; Lepage GP. In *From Actions to Answers, TASI'89*, ed. T DeGrand, D Toussaint. Singapore: World Sci. (1990)
2. Caswell WE, Lepage GP. *Phys. Lett.* B167:437 (1986)
3. Georgi H. *Phys. Lett.* B240:447 (1990)
4. Son DT, Stephanov MA. *Phys. Rev.* D61:074012 (2000); Beane SR, Bedaque PF, Savage MJ. *Phys. Lett.* B483:131 (2000); Barducci A, Casalbuoni R, Pettini G, Gatto R. *Phys. Rev.* D63:074002 (2001)
5. Manohar A, Georgi H. *Nucl. Phys.* B234:189 (1984)
6. Weinberg S. *Phys. Lett.* B251:288 (1990); *Nucl. Phys.* B363:3 (1991)
7. Ordóñez C, van Kolck U. *Phys. Lett.* B291:459 (1992)
8. Weinberg S. *Phys. Lett.* B295:114 (1992)
9. Ordóñez C, Ray L, van Kolck U. *Phys. Rev. Lett.* 72:1982 (1994); *Phys. Rev.* C53:2086 (1996)
10. van Kolck U. *Phys. Rev.* C49:2932 (1994)
11. van Kolck U. *Few-Body Syst. Suppl.* 9:444 (1995); U. of Texas Ph.D. Dissertation (1993)
12. Bedaque PF, van Kolck U. *Phys. Lett.* B428:221 (1998)
13. van Kolck U. In *Proceedings of the Workshop on Chiral Dynamics 1997, Theory and Experiment*, ed. A Bernstein, D Drechsel, T Walcher. Berlin: Springer-Verlag (1998), hep-ph/9711222.
14. van Kolck U. *Nucl. Phys.* A645:273 (1999)
15. Chen JW, Rupak G, Savage MJ. *Nucl. Phys.* A653:386 (1999)

16. Bethe HA. *Phys. Rev.* 76:38 (1949)
17. Efimov V. TPI-MINN-89-31-T.
18. van Kolck U. *Prog. Part. Nucl. Phys.* 43:337 (1999); Beane SR, Bedaque PF, Haxton WC, Phillips DR, Savage MJ. In *Boris Ioffe Festschrift*, ed. M Shifman, Singapore: World Sci. (2001), nucl-th/0008064
19. *Nuclear Physics with Effective Field Theory*, ed. R Seki, MJ Savage, U van Kolck. Singapore: World Sci. (1998); *Nuclear Physics with Effective Field Theory II*, ed. PF Bedaque, MJ Savage, R Seki, U van Kolck. Singapore: World Sci. (2000)
20. Braaten E, Nieto A. hep-th/9609047; Hammer H-W, Furnstahl R.J. *Nucl. Phys.* A678:277 (2000); Furnstahl R.J, Hammer H-W, Tirfessa N. *Nucl. Phys.* A689:846 (2001); Hammer H-W, Furnstahl R.J. nucl-th/0108069
21. Bedaque PF, Hammer H-W, van Kolck U. *Phys. Rev. Lett.* 82:463 (1999); *Nucl. Phys.* A646:444 (1999).
22. Bedaque PF, Braaten E, Hammer H-W. *Phys. Rev. Lett.* 85:908 (2000); Braaten E, Hammer H-W. *Phys. Rev. Lett.* 87:160407 (2001); Braaten E, Hammer H-W, Mehen T. *Phys. Rev. Lett.* 88:040401 (2002)
23. Kaplan DB, Savage MJ, Wise MB. *Phys. Lett.* B424:390 (1998); *Nucl. Phys.* B534:329 (1998)
24. Mehen T, Stewart IW. *Phys. Lett.* B445:378 (1999); Gegelia J. nucl-th/9802038
25. Birse MC, McGovern JA, Richardson KG. *Phys. Lett.* B464:169 (1999)
26. Stoks VGJ, Klomp RAM, Rentmeester MCM, de Swart JJ. *Phys. Rev.* C48:792 (1993)
27. Kong X, Ravndal F. *Phys. Lett.* B450:320 (1999); *Nucl. Phys.* A665:137 (2000)
28. Beane SR, Savage MJ. *Nucl. Phys.* A694:511 (2001)
29. Griebhammer HW, Rupak G. *Phys. Lett.* B529:57 (2002)
30. Riska DO, Brown GE. *Phys. Lett.* B38:193 (1972)
31. Rupak G. *Nucl. Phys.* A678:405 (2000)
32. Arenhövel H, Sanzone M. *Photodisintegration of the Deuteron: A Review of Theory and Experiment*, Berlin: Springer-Verlag (1991)
33. Chen JW, Rupak G, Savage MJ. *Phys. Lett.* B464:1 (1999)
34. Butler M, and Chen JW. *Nucl. Phys.* A675:575 (2000); Butler M, Chen JW, Kong X. *Phys. Rev.* C63:035501 (2001); Chen JW. *Nucl. Phys.* A684:484 (2001)
35. Kong X, Ravndal F. *Nucl. Phys.* A656:421 (1999); *Phys. Lett.* B470:1 (1999); *Phys. Rev.* C64:044002 (2001); Butler M, Chen JW. *Phys. Lett.* B520:87 (2001)
36. Bedaque PF, Hammer H-W, van Kolck U. *Phys. Rev.* C58:641 (1998)
37. Gabbiani F, Bedaque PF, Griebhammer HW. *Nucl. Phys.* A675:601 (2000)
38. Bedaque PF, Hammer H-W, van Kolck U. *Nucl. Phys.* A676:357 (2000)
39. Kaplan, DB *Nucl. Phys.* B494:471 (1997)
40. Mehen T, Stewart IW, Wise M. *Phys. Rev. Lett.* 83:931 (1999)
41. Amado RD. In *Elementary Particle Physics and Scattering Theory, Vol.2*, ed. M Chrétien, S Schweber. New York: Gordon and Breach (1970)
42. Skorniakov GV, Ter-Martirosian KA. *Sov. Phys. JETP* 4:648 (1957)
43. van Oers WTH, Seagrave JD. *Phys. Lett.* B24:562 (1967); Phillips AC, Barton G. *Phys. Lett.* B28:378 (1969)
44. Dilg W, Koester L, Nistler W. *Phys. Lett.* B36:208 (1971)
45. Efimov VN, Tkachenko EG. JINR-E4-8473
46. Friar JL, Hüber D, Witała H, Payne GL. *Acta Phys. Polon.* B31:749 (2000)
47. Rupak G, Kong XW. nucl-th/0108059
48. Faddeev LD, Minlos RA. *Sov. Phys. JETP* 14:1315 (1962)
49. Danilov GS. *Sov. Phys. JETP* 16:1010 (1963)
50. Efimov VN. *Sov. J. Nucl. Phys.* 12:589 (1971); 28:546 (1979); *Nucl. Phys.* A210:157 (1973); Amado RD, Noble JV. *Phys. Rev.* D5:1992 (1972)
51. Mehen T, Stewart IW, Wise MB. *Phys. Lett.* B474:145 (2000)
52. Hammer H-W, Mehen T. *Nucl. Phys.* A690:535 (2001)
53. Wilson KG. *Phys. Rev.* D3:1818 (1971); Glazek SD, Wilson KG. *Phys. Rev.* D47:4657 (1993)
54. Glazek SD, Wilson KG. hep-th/0203088
55. Hammer H-W, Mehen T. *Phys. Lett.* B516:353 (2001)
56. Bedaque PF, Griebhammer H, Hammer H-W, Rupak G. In preparation
57. Kievsky A, Rosati S, Tornow W, Viviani M. *Nucl. Phys.* A607:402 (1996); Kievsky A. Private communication (2002)
58. Phillips AC. *Nucl. Phys.* A107:209 (1968)

59. Efimov V, Tkachenko EG. *Few-Body Syst.* 4:71 (1988)
60. Efimov V, Tkachenko EG. *Phys. Lett.* B157:108 (1995)
61. Hammer H-W. nucl-th/0110031
62. Goldstone J, Salam A, Weinberg S. *Phys. Rev.* 127:965 (1962)
63. Coleman S, Wess J, Zumino B. *Phys. Rev.* 177:2239 (1969); Callan CG, Coleman S, Wess J, Zumino B. *Phys. Rev.* 177:2247 (1969)
64. Bernard V, Kaiser N, Meißner U-G. *Int. J. Mod. Phys.* E4:193 (1995)
65. Weinberg S. *Physica* 96A:327 (1979)
66. Lutz M. In hep-ph/9606301; Private communication (1996, 1997)
67. Cohen TD, Hansen JM. *Phys. Lett.* B440:233 (1998)
68. Gegelia J. nucl-th/9806028; Cohen TD, Hansen JM. *Phys. Rev.* C59:13,304 (1999)
69. Mehen T, Stewart IW. *Phys. Lett.* B445:378 (1999); *Phys. Rev.* C59:2365 (1999); *Nucl. Phys.* A665:164 (2000)
70. Steele JV, Furnstahl RJ. *Nucl. Phys.* A645:439 (1999)
71. Rupak G, Shoresh N. *Phys. Rev.* C60:054004 (1999)
72. Fleming S, Mehen T, Stewart IW. *Nucl. Phys.* A677:313 (2000); *Phys. Rev.* C61:044005 (2000)
73. Kaiser N, Brockmann R, Weise W. *Nucl. Phys.* A625:758 (1997); Kaiser N, Gerstendörfer S, Weise W. *Nucl. Phys.* A637:395 (1998); Ballot JL, Robilotta MR, da Rocha CA. *Phys. Rev.* C57:1574 (1998)
74. Coon SA, Friar JL. *Phys. Rev.* C34:1060 (1986); Friar JL. *Czech. J. Phys.* 43:259 (1993)
75. Lepage, GP. nucl-th/9706029; Gegelia J. *Phys. Lett.* B463:133 (1999)
76. Park T-S, Kubodera K, Min D-P, Rho M. *Phys. Rev.* C58:637 (1998); *Nucl. Phys.* A646:83 (1999); Hyun C-H, Min D-P, Park T-S. *Phys. Lett.* B473:6 (2000)
77. Frederico T, Timóteo VS, and Tomio L. *Nucl. Phys.* A653:209 (1999)
78. Epelbaum E, Glöckle W, Meißner U-G. *Nucl. Phys.* A671:295 (2000)
79. Frank WM, Land DJ, Spector RM. *Rev. Mod. Phys.* 43:36 (1971); Perelomov AM, Popov VS. *Teor. i. Mate. Fiz.* 4:48 (1970)
80. Beane SR, Bedaque PF, Childress L, Kryjevski A, McGuire J, van Kolck U. *Phys. Rev.* A64:042103 (2001)
81. Camblong HE, Ordóñez CR. hep-th/0110278
82. Barford T, Birse MC. nucl-th/0108024
83. Beane SR, Bedaque PF, Savage MJ, van Kolck U. *Nucl. Phys.* A700:377 (2002)
84. Sprung DWL, van Dijk W, Wang E, Zheng DC, Sarriguren P, Martorell J. *Phys. Rev.* C49:2942 (1994)
85. Kaplan DB and Steele JV. *Phys. Rev.* C60:064002 (1999)
86. Scaldeferri KA, Phillips DR, Kao C-W, Cohen TD. *Phys. Rev.* C56:679 (1997)
87. Gegelia J, Japaridze G. *Phys. Lett.* B517:476 (2001); Eiras D, Soto J. nucl-th/0107009
88. Lutz M. *Nucl. Phys.* A677:241 (2000)
89. Friar JL, Coon SA. *Phys. Rev.* C49:1272 (1994); Epelbaum E, Glöckle W, Meißner U-G. *Nucl. Phys.* A637:107 (1998); Friar JL. *Phys. Rev.* C60:034002 (1999)
90. Wiringa RB, Stoks VGJ, Schiavilla R. *Phys. Rev.* C51:38 (1995)
91. Brueckner KA, Watson KM. *Phys. Rev.* 92:1023 (1953); Sugawara M, Okubo S. *Phys. Rev.* 117:605,611 (1960); Sugawara H, von Hippel F. *Phys. Rev.* 172:1764 (1968)
92. Rentmeester MCM, Timmermans RGE, Friar JL, de Swart JJ. *Phys. Rev. Lett.* 82:4992 (1999); Timmermans RGE. Private communication (2001)
93. Epelbaum E, Meißner U-G, Glöckle W, Elster C. nucl-th/0106007
94. Entem DR, Machleidt R. *Phys. Lett.* B524:93 (2002)
95. Bogner SK, Kuo TT, Schwenk A, Entem DR, Machleidt R. nucl-th/0108041
96. Kaiser N. *Phys. Rev.* C61:014003 (2000); C62:024001 (2000); C63:044010 (2001); C64:057001 (2001); C65:017001 (2002)
97. Entem DR, Machleidt R. nucl-th/0202039
98. Miller GA, Nefkens BMK, Slaus I. *Phys. Rept.* 194:1 (1990)
99. van Kolck U, Rentmeester MCM, Friar JL, Goldman T, de Swart JJ. *Phys. Rev. Lett.* 80:4386 (1998)
100. Friar JL, van Kolck U. *Phys. Rev.* C60:034006 (1999)
101. Niskanen JA, *Phys. Rev.* C65:037001 (2002)
102. van Kolck U, Friar JL, Goldman T. *Phys. Lett.* B371:169 (1996)
103. Coon SA, McKellar BHJ, Stoks VGJ. *Phys. Lett.* B385:25 (1996)

104. Walzl M, Meißner U-G, Epelbaum E. *Nucl. Phys.* A693:663 (2001)
105. Epelbaum E, Meißner U-G. *Phys. Lett.* B461:287 (1999)
106. Pieper SC, Wiringa RB. *Ann. Rev. Nucl. Part. Sci.* 51:53 (2001)
107. Epelbaum E, Kamada H, Nogga A, Witała H, Glöckle W, Meißner U-G. *Phys. Rev. Lett.* 86:4787 (2001)
108. Entem DR, Machleidt R, Witała H. nucl-th/0111033
109. Coon SA, Scadron MD, McNamee PC, Barrett BR, Blatt DWE, McKellar BHJ. *Nucl. Phys.* A317:242 (1979); Coelho HT, Das TK, Robilotta MR. *Phys. Rev.* C28:1812 (1983)
110. Friar JL, Hüber D, van Kolck U. *Phys. Rev.* C59:53 (1999)
111. Coon SA, Han HK. *Few-Body Syst.* 30:131 (2001); Kamada H, Hüber D, Nogga A. *Few-Body Syst.* 30:121 (2001)
112. Hüber D, Friar JL, Nogga A, Witała H, van Kolck U. *Few-Body Syst.* 30:95 (2001)
113. Ellis RG, Coon SA, McKellar BHJ. *Nucl. Phys.* A438:631 (1985); Coon SA, Peña MT, Riska DO. *Phys. Rev.* C52:2925 (1995)
114. Stewart IW. Private communication (2000); Epelbaum E. Private communication (2001)
115. Beane SR, Phillips DR, Malheiro M, van Kolck U. *Nucl. Phys.* A656:367 (1999)
116. Rho M. *Phys. Rev. Lett.* 66:1275 (1991)
117. Kaplan DB, Savage MJ, Wise MB. *Phys. Rev.* C59:617 (1999); Phillips DR, Cohen TD. *Nucl. Phys.* A668:45 (2000); Walzl M, Meißner U-G. *Phys. Lett.* B513:37 (2001); Phillips DR. In *Mesons and Light Nuclei*, ed. J. Adam et al, New York: AIP Press (2001), nucl-th/0108070
118. Savage MJ, Springer RP. *Nucl. Phys.* A644:235 (1998), (E) A657:457 (1999); A686:413 (2001); Diaconescu L, Schiavilla R, van Kolck U. *Phys. Rev.* C63:044007 (2001)
119. Park T-S, Min D-P, Rho M. *Phys. Rev. Lett.* 74:4153 (1995); *Nucl. Phys.* A596:515 (1996); Savage MJ, Scaldeferri KA, Wise MB. *Nucl. Phys.* A652:273 (1999); Park T-S, Kubodera K, Min D-P, Rho M. *Phys. Lett.* B472:232 (2000); Hyun C-H, Min D-P, Park T-S. *Phys. Lett.* B473:6 (2000)
120. Kaplan DP, Savage MJ, Springer RP, Wise MB. *Phys. Lett.* B449:1 (1999); Hyun C-H, Park T-S, Min D-P. *Phys. Lett.* B516:321 (2001)
121. Park T-S, Min D-P, Rho M. *Phys. Rep.* 233:341 (1993); Park T-S, Kubodera K, Min D-P, Rho M. *Astrophys. J.* 507:443 (1998); Park T-S, Marcucci LE, Schiavilla R, Viviani M, Kievsky A, Rosati S, Kubodera K, Min D-P, Rho M. nucl-th/0106025
122. Park T-S, Marcucci LE, Schiavilla R, Viviani M, Kievsky A, Rosati S, Kubodera K, Min D-P, Rho M. nucl-th/0107012
123. Nakamura S, Sato T, Ando S, Park T-S, Myhrer F, Gudkov V, Kubodera K. nucl-th/0201062
124. Ando S, Park T-S, Kubodera K, Myhrer F. nucl-th/0109053
125. Chen JW, Griesshammer HW, Savage MJ, Springer RP. *Nucl. Phys.* A644:221,245 (1998); Chen JW. *Nucl. Phys.* A653:375 (1999)
126. Beane SR, Bernard V, Lee T-SH, Meißner U-G. *Phys. Rev.* C57:424 (1998)
127. Kaiser N. nucl-th/0203001
128. Misra A, Koltun DS. *Phys. Rev. C* 61:024003 (2000)
129. Beane SR, Bernard V, Epelbaum E, Meißner U-G, Phillips DR. In preparation
130. Rockmore RM. *Phys. Lett.* B356:153 (1995)
131. Borasoy B, Griesshammer HW. nucl-th/0105048
132. Beane SR, Lee CY, van Kolck U. *Phys. Rev.* C52:2914 (1995); Beane SR, Bernard V, Lee T-SH, Meißner U-G, van Kolck U. *Nucl. Phys.* A618:381 (1997)
133. Wilhelm P. *Phys. Rev.* C56:1215 (1997)
134. Koch JH, Woloshyn RM. *Phys. Rev.* C16:1986 (1997); Laget JM. *Phys. Rep.* 69:1 (1981)
135. Bergstrom JC, et al. *Phys. Rev.* C57:3203 (1998)
136. Levchuk MI, Schumacher M, Wissmann F. *Nucl. Phys.* A675:621 (2000)
137. Bernard V, Krebs H, Meißner U-G. *Phys. Rev.* C61:058201 (2000)
138. Ewald I, et al (A1 Collaboration). *Phys. Lett.* B499:238 (2001)
139. Cohen TD, Friar JL, Miller GA, van Kolck U. *Phys. Rev.* C53:2661 (1996)
140. Hanhart C, van Kolck U, Miller GA. *Phys. Rev. Lett.* 85:2905 (2000)
141. Bernard V, Kaiser, Meißner U-G. *Eur. Phys. J.* A4:259 (1999)
142. van Kolck U, Miller GA, Riska DO. *Phys. Lett.* B388:679 (1996); Peña MT, Riska DO, Stadler A. *Phys. Rev.* C60:045201 (1999)
143. Park BY, Myhrer F, Morones JR, Meissner T, Kubodera K. *Phys. Rev.* C53:1519 (1996);

- Sato T, Lee T-SH, Myhrer F, Kubodera K. *Phys. Rev.* C56:1246 (1997); Hanhart C, Haidenbauer J, Hoffmann M, Meißner U-G, Speth J. *Phys. Lett.* B424:8 (1998); Gedalin E, Moalem A, Razdolskaya L. *Phys.Rev.* C60:031001 (1999); Dmitrasinovic V, Kubodera K, Myhrer F, Sato T. *Phys. Lett.* B465:43 (1999); Ando S, Park T-S, Min D-P. *Phys. Lett.* B509:253 (2001)
144. da Rocha CA, Miller GA, van Kolck U. *Phys. Rev.* C61:034613 (2000)
 145. van Kolck U, Niskanen JA, Miller GA. *Phys. Lett.* B493:65 (2000)
 146. Opper AK, Korkmaz E (spokespersons). TRIUMF E-704 Proposal
 147. Bacher AD, Stephenson EJ (spokespersons). IUCF CE-82 Proposal
 148. Hanhart C, Miller GA, Myhrer F, Sato T, van Kolck U. *Phys. Rev.* C63:044002 (2001)
 149. Fukugita M, Kuramashi Y, Okawa M, Mino H, Ukawa A. *Phys. Rev.* D52:3003 (1995)
 150. Wiringa R. Private communication (2001)
 151. Beane SR, Savage MJ. hep-lat/0202013.
 152. Zheng DC, Barrett BR, Jaqua L, Vary JP, McCarthy RJ. *Phys. Rev.* C48:1083 (1993); Haxton WC, Song CL. *Phys. Rev. Lett.* 84:5484 (2000); Haxton WC, Luu T. *Nucl. Phys.* A690:15 (2001); Fayache MS, Vary JP, Barrett BR, Navratil P, Aroua S. nucl-th/0112066
 153. van Kolck U. In hep-ph/0201266; Bertulani CA, Hammer H-W, van Kolck U. In preparation
 154. Friar JL, Madland DG, Lynn BW. *Phys. Rev.* C53:3085 (1996); Furnstahl RJ and Serot BD. *Nucl. Phys.* A663:513 (2000); Steele JV. nucl-th/0010066; Brown GE, Rho M. hep-ph/0103102
 155. Müller H-M, Koonin SE, Seki R, van Kolck U. *Phys. Rev.* C61:044320 (2000); Müller H-M, Seki R. In Ref. (19).
 156. Machleidt R, Slaus I. *J. Phys.* G27:R69 (2001); Friar JL. *Nucl. Phys.* A684:200 (2001); Coon SA. nucl-th/9903033